# Faculty of Medicine and Life Sciences
## *School for Life Sciences*
Master of Biomedical Sciences

**Master's thesis**

***Echocardiographic evaluation to allow early detection of doxorubicin-induced cardiotoxicity in rats***

**Lisa Steegen**
Thesis presented in fulfillment of the requirements for the degree of Master of Biomedical Sciences, specialization
Molecular Mechanisms in Health and Disease

**SUPERVISOR :**
Prof. dr. Virginie BITO

**MENTOR :**
De heer Sibren HAESEN

Transnational University Limburg is a unique collaboration of two universities in two
countries: the University of Hasselt and Maastricht University.

**2023**
**2024**

# Faculty of Medicine and Life Sciences
## *School for Life Sciences*

Master of Biomedical Sciences

### Master's thesis

*Echocardiographic evaluation to allow early detection of doxorubicin-induced cardiotoxicity in rats*

**Lisa Steegen**
Thesis presented in fulfillment of the requirements for the degree of Master of Biomedical Sciences, specialization Molecular Mechanisms in Health and Disease

**SUPERVISOR :**
Prof. dr. Virginie BITO

**MENTOR :**
De heer Sibren HAESEN

**Echocardiographic evaluation to allow early detection of doxorubicin-induced cardiotoxicity in rats\***

Steegen L[1], Haesen S[2], Heeren E[2], Deluyker D[2] and Bito V[2]

[1]Faculty of Medicine & Life Sciences, Hasselt University, Campus Diepenbeek, Agoralaan Building D - B-3590 Diepenbeek
[2]Cardio and Organ Systems (COS) research group, Biomedical Research Institute, Hasselt University, Campus Diepenbeek, Agoralaan Building C - B-3590 Diepenbeek

\*Running title: *Early detection of DOX-induced cardiotoxicity in rats*

To whom correspondence should be addressed: Virginie Bito, Tel: +32 (11) 26 92 85; Email: virginie.bito@uhasselt.be

**ABSTRACT**

**Doxorubicin (DOX) is a frequently used chemotherapeutic agent with high antitumor efficacy but dose-dependent cardiotoxicity (1). Four-dimensional echocardiography (4DE) is the preferred method for assessing left ventricular (LV) function in rodents, with LV ejection fraction (LVEF) commonly used to detect cardiotoxicity (2). However, studies on additional echocardiographic parameters to detect LV dysfunction are lacking. This study aimed to determine the onset of DOX-induced cardiotoxicity and alternations in echocardiography parameters over time in a rat model. Moreover, we evaluated the diagnostic performance of various echocardiographic modalities and assessed interobserver consistency. Female Sprague Dawley rats received weekly intravenous injections of 2 mg/kg DOX or saline (control) for eight weeks. Transthoracic echocardiography of the LV was performed at different time points, using motion (M)-mode, brightness (B)-mode, and 4D modalities. Bias and limits of agreement were analyzed using Bland-Altman plots, while simple linear regression and Pearson correlation evaluated interobserver variability. Significant changes in LVEF, radial LV fractional shortening (LVFS), and volume parameters were observed six weeks after the first DOX injection compared to baseline, with further declines in longitudinal LVFS and LV cardiac index by week eight. B-mode echocardiography exhibited lower reproducibility for all parameters than 4D and M-mode, as indicated by higher bias and broader limits of agreement. Strong correlations were observed between researchers for most measurements. In conclusion, this study shows the time-dependent manifestation of DOX-induced cardiotoxicity in a rat model and highlights the importance of early detection and comprehensive echocardiographic assessment, with 4D and M-mode proving more reliable than B-mode.**
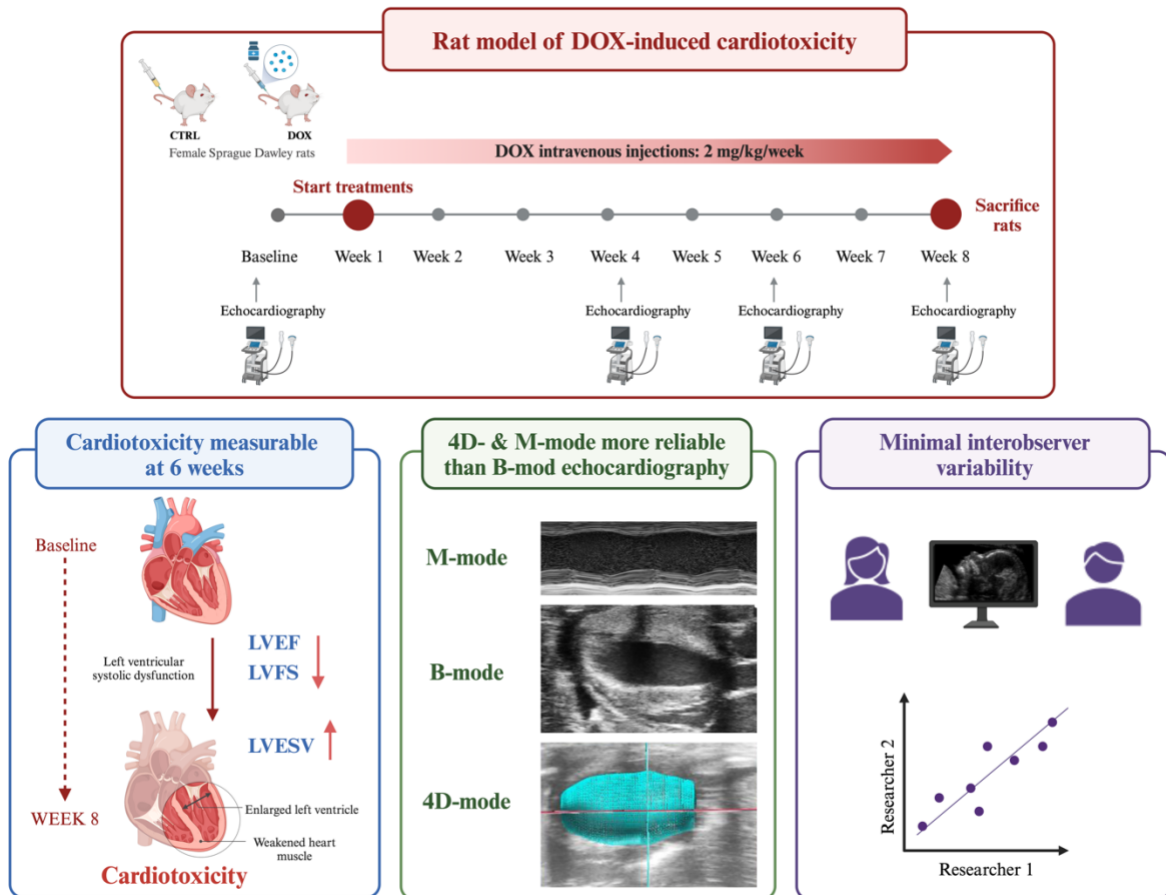
**Graphical abstract.** B-mode, brightness-mode. DOX, doxorubicin. LVEF, left ventricular ejection fraction. LVFS, left ventricular fractional shortening. LVESV, left ventricular end-systolic volume. M-mode, motion-mode. 4D-mode, four-dimensional-mode. Created with BioRender.com

## INTRODUCTION

*Anticancer treatment side effects: impact on rising cancer survivorship* – Breast cancer accounts for 13.3% of all cancer diagnoses, establishing it as the most prevalent malignancy in European women (3). In 2020, 2.26 million new cases were reported globally. Moreover, breast cancer ranks as the leading cause of cancer-related death among women worldwide (4, 5). In the last decade, there has been a notable improvement in the prognosis of breast cancer (6). This improvement can be attributed partially to earlier diagnoses (*e.g.,* screening programs) and the development of treatment advances and personalized medicine (6-8). Moreover, these advancements have led to a significant reduction in mortality rates associated with breast cancer. Conversely, the increase in survival rates has led to greater awareness of side effects that pose life-threatening risks and cause long-term morbidity. Cardiac toxicity emerges as a prominent concern associated with adjuvant

treatments for breast cancer. It is associated with an increased risk of cardiac damage, including left ventricular (LV) dysfunction, heart failure (HF), vascular disorders, arrhythmias, and ischemia (6, 9).

*Cardiotoxic adverse effects of doxorubicin* – Anthracyclines, including doxorubicin (DOX), are highly potent and widespread cytotoxic drugs used to treat various cancer types, such as leukemia, sarcomas, breast cancer, and lymphomas. Each year, approximately one million cancer patients undergo anthracycline treatment, with around 32% of breast cancer patients (10, 11). The successful use of DOX has been hindered by its dose-dependent, irreversible cardiotoxic side effects, which may occur during treatment or persist for many years after chemotherapy cessation (1, 11). For example, DOX is associated with a 5% incidence of congestive heart failure when a cumulative lifetime dose of 400 mg/m$^2$ is reached, and higher doses lead to

an exponential increase in risk, up to 48% at 700 mg/m$^2$ (12). Several definitions exist for diagnosing cardiotoxicity. Additionally, pre-existing heart conditions, established cardiovascular risk factors, female sex, and age are significant factors that influence the development of DOX-induced cardiotoxicity (12, 13). In addition, approximately 15% of patients treated with anthracyclines die because of cardiovascular diseases (CVD) (14, 15). This highlights a major concern in the field of cardio-oncology due to its comparable risk to cancer mortality itself (16).

*Mechanisms of DOX-induced cardiotoxicity* – DOX uses multiple molecular mechanisms to disrupt tumor growth. On one side, DOX can induce DNA damage by elevating the production of reactive oxygen species (ROS), resulting in oxidized nucleotides, base mismatches, point mutations, and single-strand breaks in the DNA (17). On the other hand, it intercalates into DNA, forming bulky adducts and crosslinks that disrupt DNA replication and transcription. DOX blocks the function of topoisomerase II (TOP2), which is essential for DNA replication. In this way, it interferes with the helical unwinding of DNA and activates a DNA damage response, which leads to apoptosis (17-19). There are two forms of TOP2, namely TOP2$\alpha$ and TOP2$\beta$. TOP2$\alpha$ is overexpressed in rapidly dividing cells, like tumor cells, and TOP2$\beta$ is expressed in various tissues, including cardiomyocytes (20). Due to the highly elevated expression of TOP2$\alpha$ in cancer cells, DOX treatment has a high efficacy. Nonetheless, DOX induces cardiotoxicity by inhibiting TOP2$\beta$, ultimately leading to cardiomyocyte death (18). The increase in oxidative stress arising from the imbalance between ROS and antioxidants has been suggested as a secondary mechanism contributing to the cardiotoxic effects of DOX. The formation of ROS is induced by the reduction of DOX to a semiquinone form, catalyzed by mitochondrial NADH dehydrogenase and P450 reductase. Semiquinone can readily react with oxygen to generate superoxide anions ($O_2^{\bullet-}$), which may further transform into other ROS or reactive nitrogen species. This redox cycling process amplifies oxidative stress production (19, 21, 22). Since cardiomyocytes contain a high concentration of mitochondria, a major subcellular target of DOX (21). Furthermore, DOX induces iron accumulation in the mitochondria, disrupting iron homeostasis and increasing ROS production (23). In the presence of iron, DOX can form Fe$^{3+}$-DOX complexes, which catalyze Fenton's reaction. This reaction converts hydrogen peroxide (H$_2$O$_2$) into various ROS species, including the highly reactive and cytotoxic hydroxyl radicals (OH$^-$) (19). Ultimately, this can result in lipid peroxidation-dependent ferroptosis, a form of iron-dependent programmatic cell death (24, 25). DOX-induced cardiotoxicity leads to structural abnormalities such as myofibrillar disorganization and mitochondrial decay in cardiomyocytes, resulting in apoptosis (23). Consequently, the heart undergoes structural changes characterized by a weakened heart muscle, an enlarged LV, and a reduced LV ejection fraction (LVEF) of >5% in symptomatic patients (or >10% reduction in asymptomatic patients) (26, 27). Ultimately, this can result in cardiac dysfunction, such as HF, cardiac arrhythmias, and adverse vascular events (9, 26, 28).

*Current therapies to counter cardiotoxicity* – To date, there is no adequate therapy to overcome DOX-induced cardiotoxicity or to protect the cardiovascular system. However, studies have investigated less toxic alternatives such as liposomal-encapsulated DOX, cardiovascular drugs, and coadministration of other therapeutics (29, 30). Despite these efforts, these therapeutics do not provide cardioprotective against DOX-induced cardiotoxicity. In addition, cardioprotective approaches have been investigated, including monitoring of cardiac function and dose reductions of DOX to reduce the frequency of cardiac events linked to DOX chemotherapy. Still, some patients who receive low or moderate anthracycline doses experience HF (29). Dexrazoxane (DRZ) is the only drug demonstrated to have protective effects in preclinical and clinical settings (31). Concerns regarding the interference of DRZ with the antitumor activity of DOX, a higher incidence of secondary cancers, and the high cost have restricted the use of DRZ in clinical settings (29, 30, 32). In conclusion, DOX is still the most effective chemotherapy for breast cancer patients as it increases patients' life expectancy. Therefore, it is undeniable that preventing or

reducing the risk of cardiotoxicity is crucial from a therapeutic perspective. A strategy that prevents or diminishes the risk of cardiotoxicity without impairing the effectiveness of DOX chemotherapy continues to be a major challenge. Moreover, research has demonstrated that the sensitivity and efficacy of cardioprotective therapy diminish as the time interval between the onset of cardiotoxicity and the initiation of therapy increases (33). Consequently, it is essential to develop effective strategies for early detection of cardiac damage and accurate monitoring of DOX-induced cardiotoxicity (34).

*Detection of cardiotoxicity* – Identifying myocardial damage in its subclinical phase is crucial to prevent myocyte loss. It could limit the development of irreversible cardiac injury, increasing the survival of cancer patients (35). Echocardiography is the most applied technique to detect cardiotoxicity before, during, and after anthracycline therapy by measuring LVEF. This non-invasive method thoroughly evaluates the cardiac systolic function, diastolic function, volumes, and wall motion abnormalities (36). Two-dimensional echocardiography (2DE) is the most prevalent method for assessing LVEF in cancer patients at cardiotoxicity risk. It is an effective method to safely detect LVEF with high repeatability and wide availability. Furthermore, it is relatively inexpensive compared to other imaging techniques, such as cardiac magnetic resonance (CMR). The major limitation of this technique is the lack of sensitivity in detecting subclinical myocardial injury. Additionally, poor image quality, inadequate apex visualization, LV geometric assumptions, and abnormalities in regional wall motion are other limitations (36-38). Currently, three-dimensional echocardiography (3DE) is used; here, no geometric assumptions are made (37). Moreover, relative to traditional 2DE approaches, this method has lower temporal variability and improved intra- and interobserver consistency. In contrast, 3DE is expensive and has limited availability (39). However, cardiac injury can appear before a decrease in LVEF is measurable. Therefore, utilizing LVEF as the single echocardiography parameter is insufficient to diagnose cardiotoxicity at an early stage (40). New evaluation methods, including global longitudinal strain (GLS), assessment of right ventricular (RV) function, and myocardial work (MW), all report earlier identification of cardiac dysfunction (41). However, in preclinical studies, echocardiography is the preferred method for assessing cardiac function in rodents and evaluating the LV function in case of cardiotoxicity. Similar to its application in humans, echocardiography offers the advantages of being non-invasive, safe, reproducible, readily accessible, and cost-effective (42). Four-dimensional echocardiography (4DE) is the primary choice for evaluating LV function in rodents, and LVEF is the most commonly used parameter to detect DOX-induced cardiotoxicity (2). However, like LVEF in humans, there is an urgent need for other parameters to detect myocardial changes early. To date, there has been a lack of other echocardiographic parameter studies to detect LV dysfunction during DOX treatment in rodents.

To further study the onset and progression of DOX-induced cardiotoxicity and to identify echocardiographic parameters for early detection of cardiotoxicity, we employed different echocardiography modalities in an experimental rat model of DOX-induced cardiotoxicity. In our study, we evaluated the onset of DOX-induced cardiotoxicity and alternations in echocardiography parameters over time. Moreover, we aimed to evaluate the diagnostic performance of different echocardiographic modalities and assess echocardiographic consistency between two researchers. Based on our study objectives, we hypothesize that DOX-induced cardiotoxicity is detectable by changes in multiple systolic and volume echocardiographic parameters before the final DOX injection at eight weeks. Additionally, we propose that 4DE will prove to be the most reliable and preferred method for these assessments. We expect minimal interobserver variability in echocardiographic measurements across all modalities.

**EXPERIMENTAL PROCEDURES**
*Animal experiments* – All animal experiments were conducted according to EU Directive 2010/63/EU for animal testing and approved by the local ethical committee (Ethical Commission for Animal Experimentation, UHasselt, Diepenbeek, Belgium, ID 201942 and ID 202154). The

animals received a standard pellet diet and water with *ad libitum* access. Rats were group-housed in standard cages with cage enrichment at the conventional animal facility of UHasselt. The environmental conditions were rigorously controlled, with a constant temperature of 22 °C and humidity levels maintained within the 22–24% range.

*Study design* – Six-week-old Female Sprague Dawley rats (Janvier Labs, Le Genest-Saint-Isle, France) were randomly divided into two groups. The first group received DOX (N = 14, 2 mg/kg intravenously, sourced from Accord Healthcare B.V., Utrecht, The Netherlands) once a week for eight weeks (with a cumulative dose of 16 mg/kg). The second group received an equivalent volume of 0.9% saline (CTRL; N = 14) once a week for eight weeks. The protocol and cumulative dose employed for inducing chronic DOX cardiotoxicity adhere to current guidelines for preclinical models in cardio-oncology (43). Transthoracic echocardiography was conducted at baseline, and four, six, and eight weeks after treatment initiation to evaluate LV parameters. Subsequently, the animals were sacrificed using an overdose of sodium pentobarbital (150 mg/kg intraperitoneal, Dolethal, Val d' hony Verdifarm, Beringen, Belgium).

*Echocardiography* – Rats were anesthetized with 2% isoflurane supplemented with oxygen. *In vivo* cardiac function was assessed by transthoracic echocardiography using a Vevo® 3100 high-resolution imaging system equipped with a 21-MHz transducer (FUJIFILM Visual- Sonics, Inc., Amsterdam, The Netherlands) at baseline, and four, six and eight weeks after the first DOX injection, conforming to Zacchigna *et al.*'s standards (42). The thoracic region of the rats was shaved. Depilatory cream was administered to prevent artifacts from hair. Subsequently, the rats were positioned in a supine position. The vital physiological parameters (including heart rate, respiratory rate, body temperature, and ECG signals) were non-invasively monitored using the provided Vevo Imaging Station. Both parasternal long-axis and short-axis views at the mid-ventricular level were obtained using brightness (B)-mode and motion (M)-mode. Additionally, 4DE images and apical four-chamber views were captured. M-mode images

from the parasternal short-axis were obtained to measure LV anterior and posterior ventricular wall thickness, longitudinal and radial LV fractional shortening (LVFS), and LV internal diameters in systole and diastole to calculate systolic and volume parameters. LV end-systolic and end-diastolic areas were determined from parasternal long-axis views in B-mode (EKV) by tracing the LV endocardial border during end-systole and end-diastole. Based on these parameters, other systolic and volume parameters can be measured. 4D views were utilized to measure LV end-systolic and end-diastolic volumes (LVESV and LVEDV), LV stroke volume (LVSV), LVEF, and LV cardiac output (LVCO). LVSV and LVCO were normalized to body surface area (BSA) and presented as the LVSV index and LV cardiac index. Mitral flow was evaluated from apical four-chamber views in B-mode using Pulsed-Wave (PW) Doppler mode to estimate diastolic function and calculate the E/A ratio of peak flow velocity in early versus late filling. Tissue Doppler mode assessed peak septal mitral annulus velocity in the early filling phase (E′), with measurements averaged from at least two cycles. The peak mitral flow- to annular velocity (E/E′) ratio was subsequently calculated. Analyses were performed using Vevo® LAB (Vevo® LAB software, version 5.6.1, FUJIFILM VisualSonics, Inc.). Two blinded researchers independently analyzed all echocardiographic images.

*Statistical analysis* – Statistical analysis was performed using GraphPad Prism (GraphPad Software, version 10.2.0, San Diego, CA, USA). The normal distribution of data was assessed using the D'Agostino & Pearson normality test. For parameters measured at multiple time points, the data were compared with repeated measures, mixed-effects analysis followed by the Bonferroni post hoc test. To compare the different echocardiography modes (4DE, M- and B-mode) at eight weeks, the data were compared with the parametric one-way ANOVA test followed by the Bonferroni post hoc test. Bland-Altman plots were generated to assess the agreement of measurement and reproducibility of systolic and volume functions among the three echocardiographic modes, calculating the bias with corresponding limits of agreement (95% SEM of the mean difference).
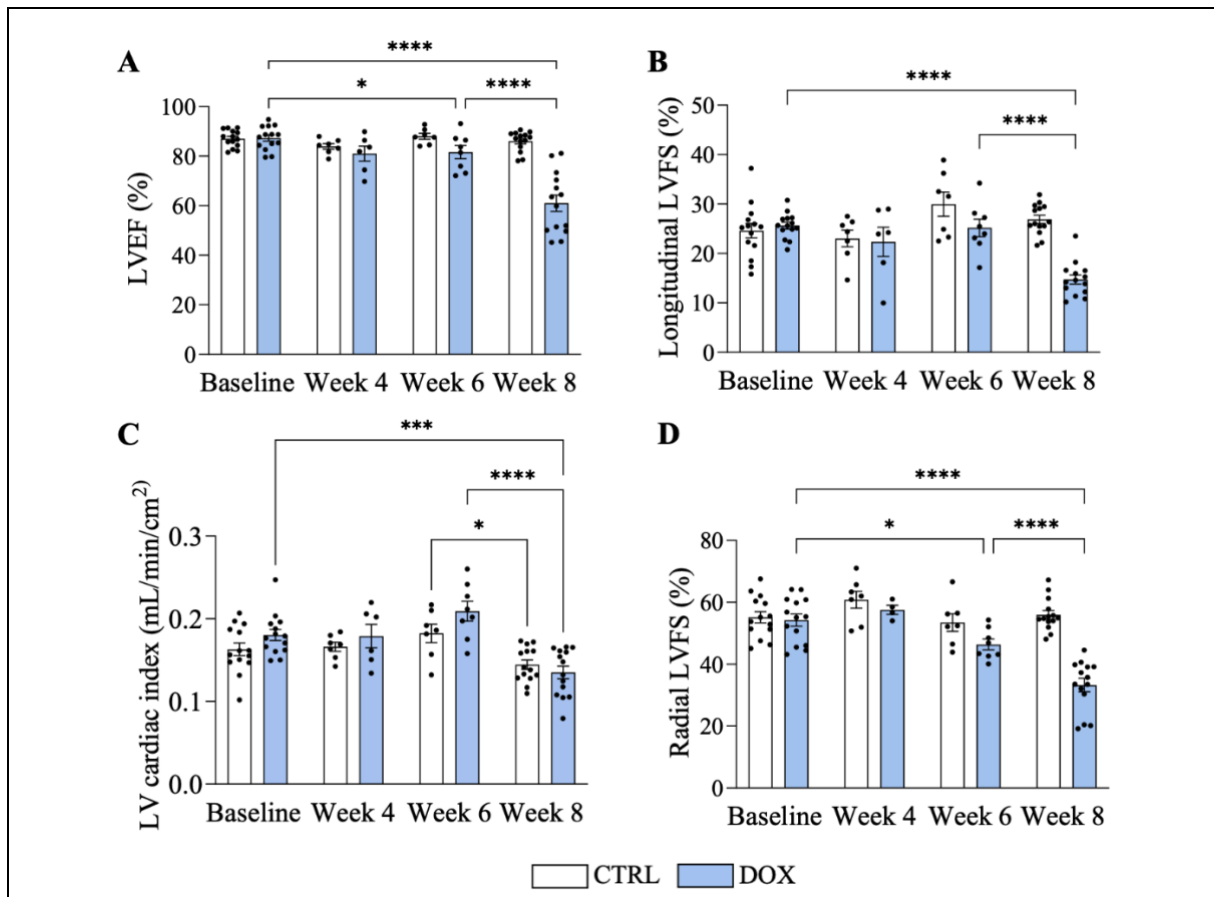
**Fig. 1 – LVEF and radial LVFS are reduced after six weeks post-DOX treatment. (A-D)** LVEF **(A)**, longitudinal LVFS **(B)**, LV cardiac index **(C)**, and radial LVFS **(D),** at baseline, weeks 4, 6, and 8 in CTRL (N=14) and DOX (N=14) animals. LVEF and LV cardiac index were measured with 4D-mode. Longitudinal and radial LVFS were measured with PSLAX B-mode and PSSAX M-mode, respectively. The LV cardiac index represents the cardiac output normalized to the body surface area (BSA). Data are presented as mean ± SEM. *$p<0.05$, **$p<0.01$, ***$p<0.001$, ****$p<0.0001$. LV, left ventricle. LVEF, left ventricular ejection fraction. LVFS, left ventricular fractional shortening.

For every Bland-Altman plot, the difference between the two methods is assessed in relation to the mean value of the parameter of interest measured by the two methods. For normally distributed data, an unpaired t-test was used to compare the data of researchers one and two. Correlation between continuous variables was evaluated using Pearson's correlation test. Correlation coefficients (r) were computed, and variables were fitted as linear regression curves. The choice to perform these statistical tests to assess reproducibility was based on the practical guide to assess the reproducibility of echocardiographic measurements (44). Outliers were detected utilizing the ROUT method, aiming for a maximum desired False Discovery Rate of 1%, adhering to this criterion established *a priori*. All data are presented as mean ± standard error of the mean (SEM). Statistical significance was defined as p<0.05.

**RESULTS**

*DOX cardiotoxicity manifests at six weeks, with increased discernibility after eight weeks for systolic and volume functions* – To examine the onset timing of DOX-induced cardiotoxicity and alternations in echocardiography parameters over time, echocardiography assessments were conducted at different time points. At baseline, cardiac parameters of DOX-treated rats were comparable to CTRL (Figures S1 & S2). At six weeks post-treatment, DOX significantly decreased left LVEF (*p<0.05*) and radial LVFS (*p<0.05*), while longitudinal LVFS and LV cardiac index did not change compared to CTRL (Figure 1). At week 8, DOX significantly reduced all systolic function parameters (*p<0.0001* for LVEF, longitudinal and radial LVFS, and *p<0.001* for LV cardiac index) (Figure 1).
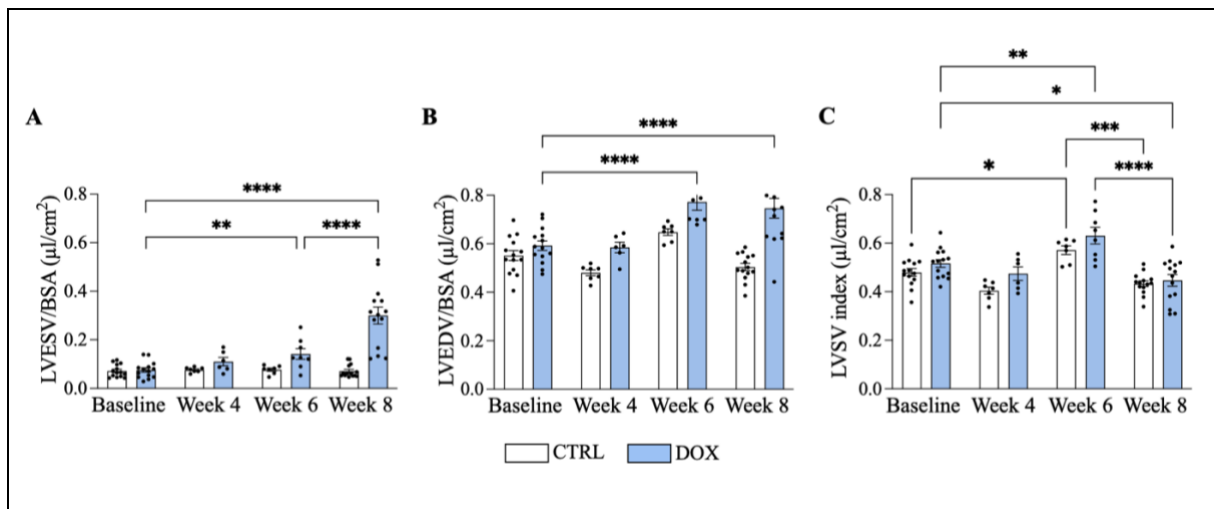
**Fig. 2 – LVSV index and LVEDV reveal increased heart volumes following six weeks of DOX treatment. (A-C)** LVESV/BSA **(A)**, LVEDV/BSA **(B)**, and LVSV index **(C)** at baseline, weeks 4, 6, and 8 in CTRL (N=14) and DOX (N=14) animals. LVESV, LVEDV, and LVSV index were measured with 4D-mode. The LVSV index represents by LVSV normalized to the body surface area (BSA). LVESV and LVEDV were also normalized to BSA. Data are presented as mean ± SEM. *$p<0.05$, **$p<0.01$, ***$p<0.001$, ****$p<0.0001$. LVESV, Left ventricular end-systolic volume. LVEDV, Left ventricular end-diastolic volume. LVSV, Left ventricular stroke volume.

Concerning volume parameters, after six weeks, for the DOX group, a significant rise in all parameters, LVESV and LVEDV ($p<0.0001$), and LVSV index ($p<0.01$) was observed (Figure 2). Furthermore, regarding systolic function, no significant differences between CTRL and DOX groups were observed before eight weeks (Figure 1S). After eight weeks of treatment, DOX-treated rats presented a 29% reduction in LVEF ($p<0.0001$), a 45% reduction in longitudinal LVFS ($p<0.0001$), and a 40% reduction in radial LVFS ($p<0.0001$) compared to CTRL (Figure S1 A-B & D). Considering volume function, after six and eight weeks of treatment, LVESV and LVEDV increased in the DOX group compared to CTRL (Figures S2 A & B). Diastolic function (E/A and E/E') was unchanged following eight weeks of DOX administration (Figure S3). Representative echocardiographic pictures of M-mode, B-mode, and 4D-mode for CTRL and DOX animals at eight weeks are shown in Figure S4.

*B-mode echocardiography exhibits significantly inferior reproducibility for systolic and volume functions.* – To evaluate differences in measurements and reproducibility of systolic and volume functions among the three echocardiographic modes, Bland-Altman plots were created. Our results pertaining to systolic function indicate that the three echo modalities exhibit comparable results when assessing LVEF and LVCO (Figure 3A&E). Regarding LVEF, the bias of all compared modes closely approaches zero with narrow limits of agreement. This indicates a high level of reproducibility between the two modes in each instance, although the bias of B-mode is higher (Figure 3B-D). Furthermore, regarding LVCO, B-mode shows broad limits of agreement compared to M-and 4D-mode, and the bias in B-mode comparisons is higher (Figure 3F-H). Comparing the various echo modes for volume parameters, a pronounced and significant difference emerges between B-mode and M-mode concerning LVSV ($p<0.05$) and LVEDV ($p<0.01$) (Figure 4A&E), a distinct trend is observed for LVESV ($p=0.07$) (Figure 4I). In relation to LVSV, all Bland-Altman plots consistently exhibit wide limits of agreement and substantial bias (Figure 4B-D). Notably, B-mode stands out, particularly when compared to 4D mode, in which the limits of agreement are markedly high. Moreover, a greater bias is observed in comparisons involving B-mode (Figure 4C-D). For LVESV, the limits of agreement are widest in B-mode versus 4D-mode comparison (Figure 4G). Substantial bias is evident in B-mode comparison with both 4D-and M-mode (Figure 4G&H).
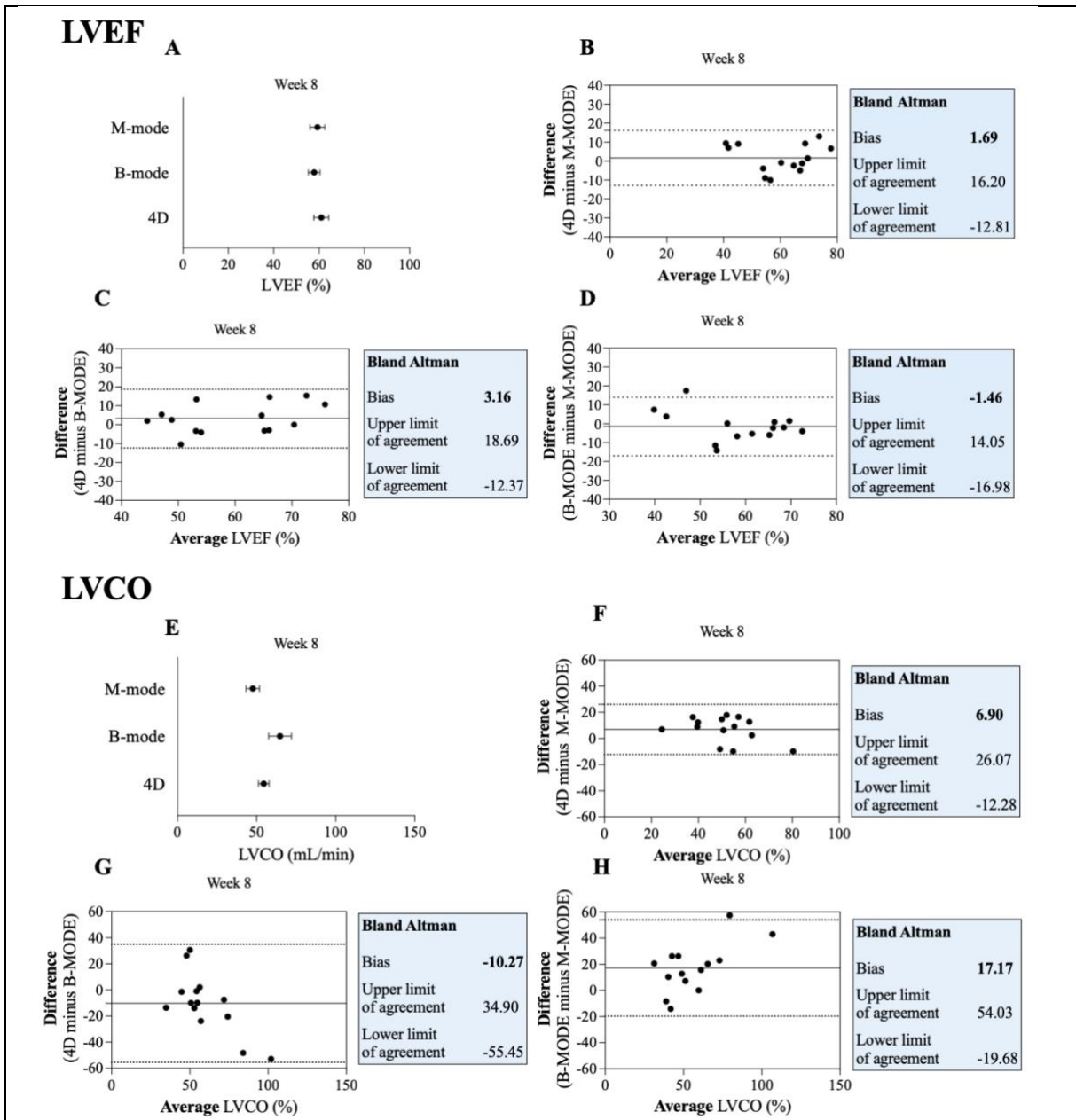
**Fig. 3 – 4D mode has the strongest reproducibility in the echocardiography measurement for systolic function (A-H).** Comparison of LVEF (**A**) and LVCO (**E**) for different echo modes, 4D, B-mode, and M-mode. Bland-Altman plots of LVEF (**B-D**) and LVCO (**F-H**) for agreement between different echo modes. Difference between 4D and M-mode for LVEF (**B**) and LVCO (**F**), the difference between 4D and B-mode for LVEF (**C**) and LVCO (**G**), and the difference between B-mode and M-mode for LVEF (**D**) and LVCO (**H**). The mean value is shown with the full line, and the Bland-Altman limits of agreements are shown with the dotted line. All measurements were performed with DOX-treated animals (N=14), after 8 weeks of treatment. Data are presented as mean ± SEM. LVCO, Left ventricular cardiac output. LVEF, Left ventricular ejection fraction.

Similar findings are observed in LVEDV but are even more pronounced (Figure 4J-L). In the comparison between 4D and B-mode, the limits of agreement are notably wide (Figure 4K). Additionally, in all three comparisons, the bias is considerably high (Figure 4J-L).

*Minimal interobserver variability in systolic and volume measurements* – Another crucial aspect to consider when assessing reproducibility is the variability between researchers. To explore this, correlation plots for systolic and volume measurements were generated between two researchers.
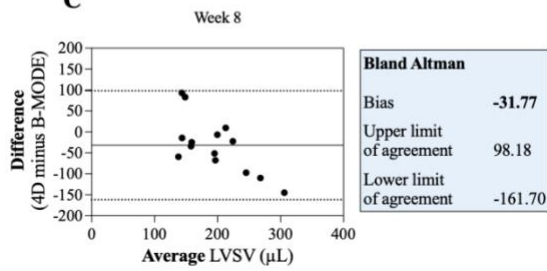
---
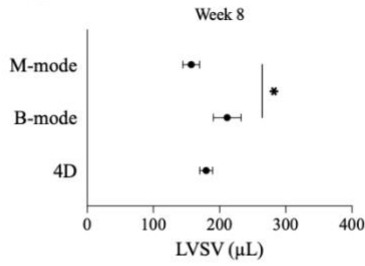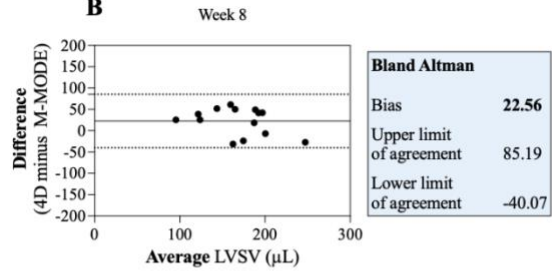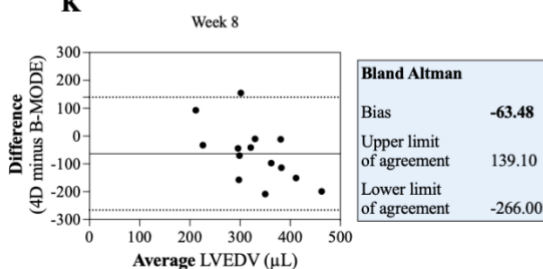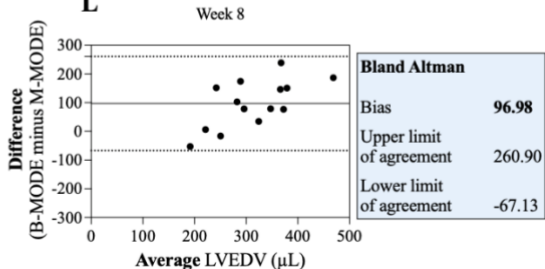
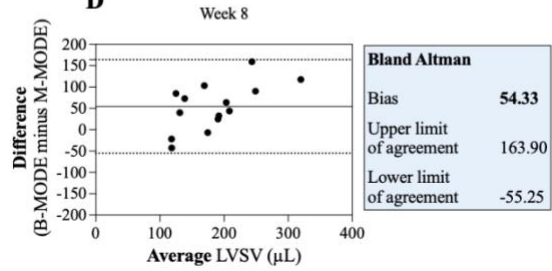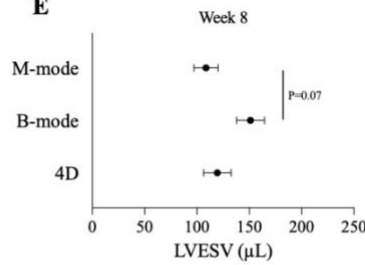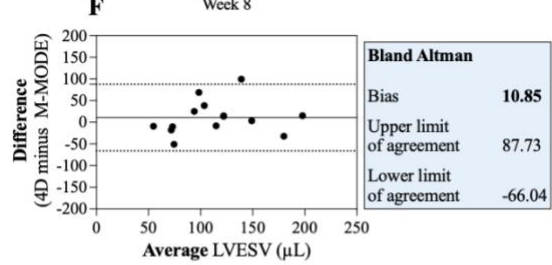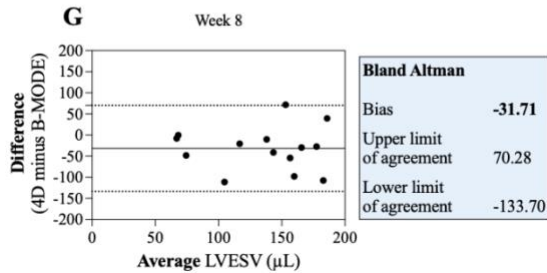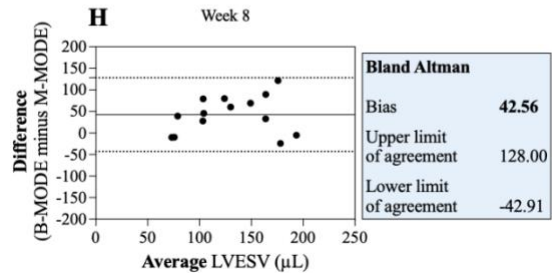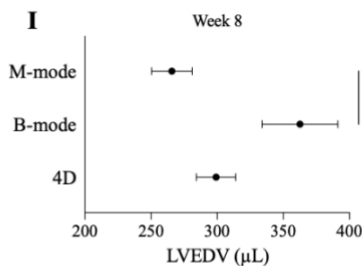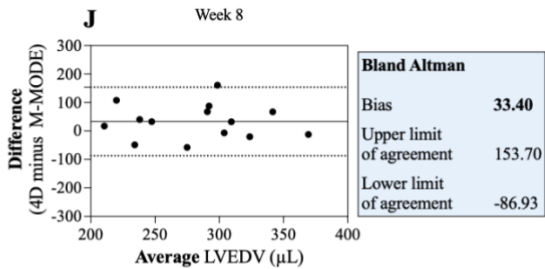**Fig. 4 – M-mode emerges as a more dependable method than B-mode for volumetric measurements (A-L).** Comparison of LVSV **(A)**, LVESV **(E)** and LVEDV **(I)** for different echo modes, 4D, B-mode, and M-mode. Bland-Altman plots of LVSV **(B-D)**, LVESV **(F-H)**, and LVEDV **(J-L)** for agreement between different echo modes. Difference between 4D and M-mode for each volume parameter **(B, F, J)**, the difference between 4D and B-mode for each volume parameter **(C, G, K)**, the difference between B-mode and M-mode for each volume parameter **(D, H, L)**. The mean value is shown with the full line, and the Bland-Altman limits of agreements are shown with the dotted line. All measurements were performed with DOX animals (N=14) 8 weeks after treatment. Data are represented as mean ± SEM. *$p<0.05$, **$p<0.01$. LVSV, Left ventricular stroke volume. LVESV, Left ventricular end-systolic volume. LVEDV, Left ventricular end-diastolic volume.

---

No significant differences between the researchers were observed (Figure 5A, C&G), except for longitudinal LVFS ($p<0.05$) (Figure 5E). Furthermore, for almost all systolic parameters, the correlation coefficient (r) ranged from 0.79 and 0.93, signifying a highly robust correlation (Figure 5B, D&H). Only longitudinal LVFS had an r-value of 0.12, indicating a weak correlation (Figure 5F). Volume assessments showed no disparity between the two researchers (Figure 6A, C&E). Similarly, the correlation coefficients ranged from 0.74 to 0.97, indicating a powerful correlation (Figure 6B, D&F).

## DISCUSSION

Although anthracyclines, including DOX, are widely used as an anticancer chemotherapeutic drug, their clinical application is limited due to cumulative dose-related cardiotoxicity (1). DOX causes myocyte injury, resulting in cardiac dysfunction, such as HF (6). Early detection of DOX-induced myocardial dysfunction is crucial to increase the survival of cancer patients. To date, echocardiography measurement of LVEF is the most common technique to detect cardiotoxicity. However, LVEF remains insensitive in identifying the first indication of myocardial damage (36). This study shows that DOX-induced cardiotoxicity can be detected six weeks after the first DOX injection, with a dose of 12 mg/kg, by a reduced LVEF, LVFS, LVESV, LVEDV, and LVSV index, intensifying by eight weeks of treatment with a dose of 16 mg/kg DOX. Furthermore, compared to M-mode and 4D-mode, B-mode echocardiography demonstrated significant variability, which reduced its reliability for evaluating LV systolic function and volumes. Lastly, except for longitudinal LVFS, strong correlations were observed in systolic and volume measurements among two researchers.

*Cardiotoxicity detection encompasses multiple parameters in addition to LVEF* – Six-week-old Female Sprague Dawley rats were weekly treated with DOX (2 mg/kg) or saline solution intravenously for eight weeks. The cumulative DOX dose of 16 mg/kg corresponds to the clinically relevant dose of 592 mg/m² given to cancer patients (45). This choice also facilitates comparison with future studies employing a model of combined breast cancer and DOX-induced cardiomyopathy, as well as addresses the underrepresentation of females in preclinical research. Consistent with clinical observations (9, 46), we observed a dose-dependent cardiotoxicity in our rats after eight weeks of DOX treatment. This was noted as LV dilated cardiomyopathy and characterized by elevated LV volumes, a decrease in stroke volume index, and a decline in all systolic parameters (LVEF, longitudinal and radial LVFS, and LV cardiac index). These results resemble the clinical phenotype of DOX-treated patients and show the reliability and translatability of our DOX-induced cardiotoxicity rat model. However, this study aimed not only to confirm the occurrence of cardiotoxicity in our rat model but also to determine the onset of DOX-induced cardiotoxicity. LVEF is described as the standard echocardiography parameter to detect cardiotoxicity. Here, we aimed to identify alternations in other systolic, diastolic, and volumetric parameters over time. Our data indicate that DOX-induced systolic and volume function impairment manifests as early as six weeks with a dose of 12 mg/kg DOX for most parameters, with increased discernibility observed after the last DOX injection with a final dose of 16 mg/kg at eight weeks. This demonstrates that echo parameters can reveal DOX-induced cardiotoxicity even before DOX treatment is completed.
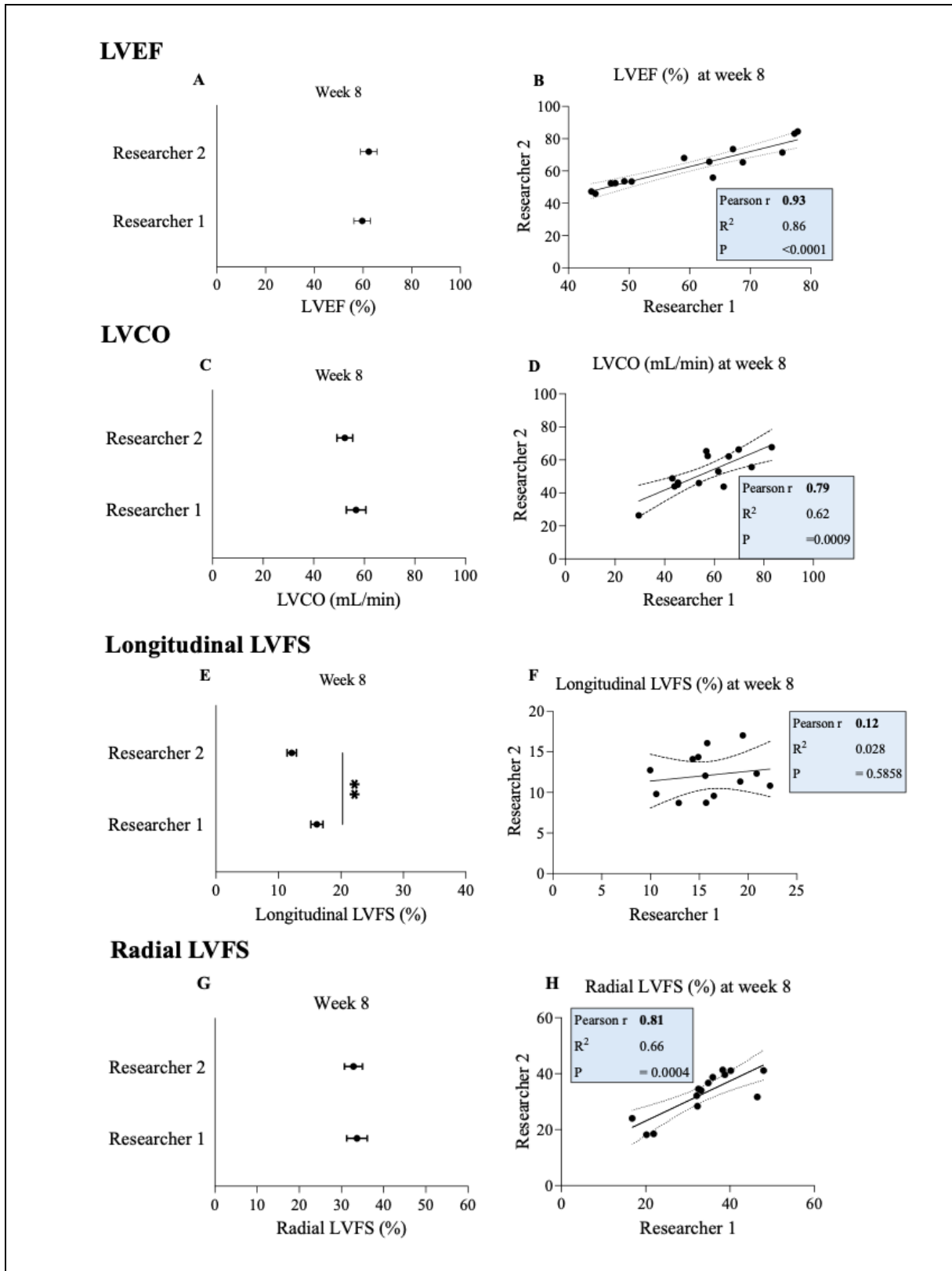
**Fig. 5 – Variation between the two researchers is evident in longitudinal LVFS measurement for systolic function. (A-H)** Comparison between researchers 1 and 2 for LVEF **(A)**, LVCO **(C)**, longitudinal LVFS **(E),** and radial LVFS **(G)**. Correlation between researchers 1 and 2 for LVEF **(B)**, LVCO **(D)**, longitudinal LVFS **(F),** and radial LVFS **(H)**. All measurements were performed with DOX animals (N=14) 8 weeks after treatment. Data are represented as mean ± SEM. *$p<0.05$. LVCO, Left ventricular cardiac output. LVEF, Left ventricular ejection fraction. LVFS, Left ventricular fractional shortening.

Chan *et al.* also showed this systolic and volumetric impairment when treating male mice once a week for four weeks with a cumulative dose of 24 mg/kg with DOX. After 28 days, DOX decreased LVFS, LVEF, and LVCO and increased LVESV relative to control (47). Multiple studies have reported a decline in LVEF, either after eight weeks when a cumulative dose of 2.5 mg/kg/week for eight weeks was given or after five weeks with a cumulative dose of 16 mg/kg for four weeks (34, 48). Xiang *et al.* demonstrated a decrease in LVCO in DOX-treated rats after six weeks with a dose of 15 mg/kg DOX compared to control, and a decline in LVFS was seen after nine weeks. The rats received 2.5 mg/kg DOX weekly for six weeks (49). Another study that treated rats with a dose of 1.5 mg/kg weekly for eight weeks showed a reduced LVFS after nine weeks of DOX treatment with a total dose of 12 mg/kg. No differences were detected at six weeks with a dose of 9 mg/kg DOX (50). Nevertheless, some studies did not find an impaired systolic function after eight weeks. For example, Chakouri *et al.* showed a decrease in LVEF and LVFS one month after the last injection. Rats were treated with cumulative doses of DOX (7.5, 10, or 12.5 mg/kg) once a week for six weeks (51). Two other studies reported no differences in LVEF and LVFS, their treatment periods were three and four weeks, with treatment doses of 3 mg/kg twice a week and 10 mg/kg/week, respectively (52, 53). The study of McLean *et al.* showed a reduction in LVSV after six weeks with a cumulative dose of 40 mg/kg DOX (53). Regarding diastolic function, our findings showed no changes in E/A and E/E' after DOX treatment. Notwithstanding, given that diastolic function precedes systolic dysfunction, the literature suggests conducting a comprehensive evaluation of diastolic function. A change in diastolic function was seen by the reduction in E'/A' or E/E' in DOX-treated animals compared to controls in multiple studies (34, 47). Our divergent results may be elucidated by the higher cumulative doses of DOX used in other studies, suggesting that changes in diastolic function might only occur after a certain dose of DOX. Additionally, it has not been demonstrated in either preclinical or clinical studies that DOX causes changes in LV diastolic function (54). Lastly, echocardiographic parameters of diastolic function are influenced by variations in cardiac

load, cardiac rhythm, age, and differences in measurement techniques, which could explain the opposing findings within different studies (55). While our findings align with some studies, discrepancies with others may be explained by variations in cumulative dose and time intervals at which DOX was administered across the various studies. Moreover, it is important to note that our study performed 4DE, whereas other studies employed M-mode or B-mode. Research has shown that 4DE is significantly more accurate with much lower temporal variation as there is no need for geometric assumptions (42, 56). Furthermore, Stegmann *et al.* demonstrated that results provided with 4DE are as precise as 4D CMR and highly reproducible, suggesting that 4DE can be seen as the method of choice for cardiac imaging (57). Differences in results may be due to variations in sample size, body weight, dose factors, subject species, or treatment regimen. A higher dose of DOX over a short period of time gives rise to acute myocardial stress and dysfunction. Whereas a lower dose over a more extended time period leads to congestive heart failure (58, 59). Chronic cardiotoxicity is characterized by changes in LV geometry, characterized by thinning of the ventricular wall, and dilation of the ventricular chamber. Altogether, our study shows that chronic cardiotoxicity can be demonstrated in week six after a cumulative dose of 12 mg/kg DOX using echocardiography. In addition to LVEF, changes in LVFS and LVCO index regarding systolic function and LVESV regarding volume function can also serve as functional parameters to detect early DOX cardiotoxicity in preclinical models when using 4DE.

*B-mode echocardiography is not as reproducible as previously thought* – Echocardiography offers a reliable, cost-effective, and widely accessible technique for evaluating cardiac function in both human and small animal imaging (60). Multiple echocardiography modalities, M-mode, B-mode, and 3D/4D mode, are available to determine the heart function. The prevailing choice for evaluating LV systolic and volume functions is 4DE (2). However, there is a shortage of direct comparisons among 4DE, B-mode, and M-mode for various systolic, diastolic, and volume parameters, particularly regarding reproducibility and variability in DOX-induced rats.
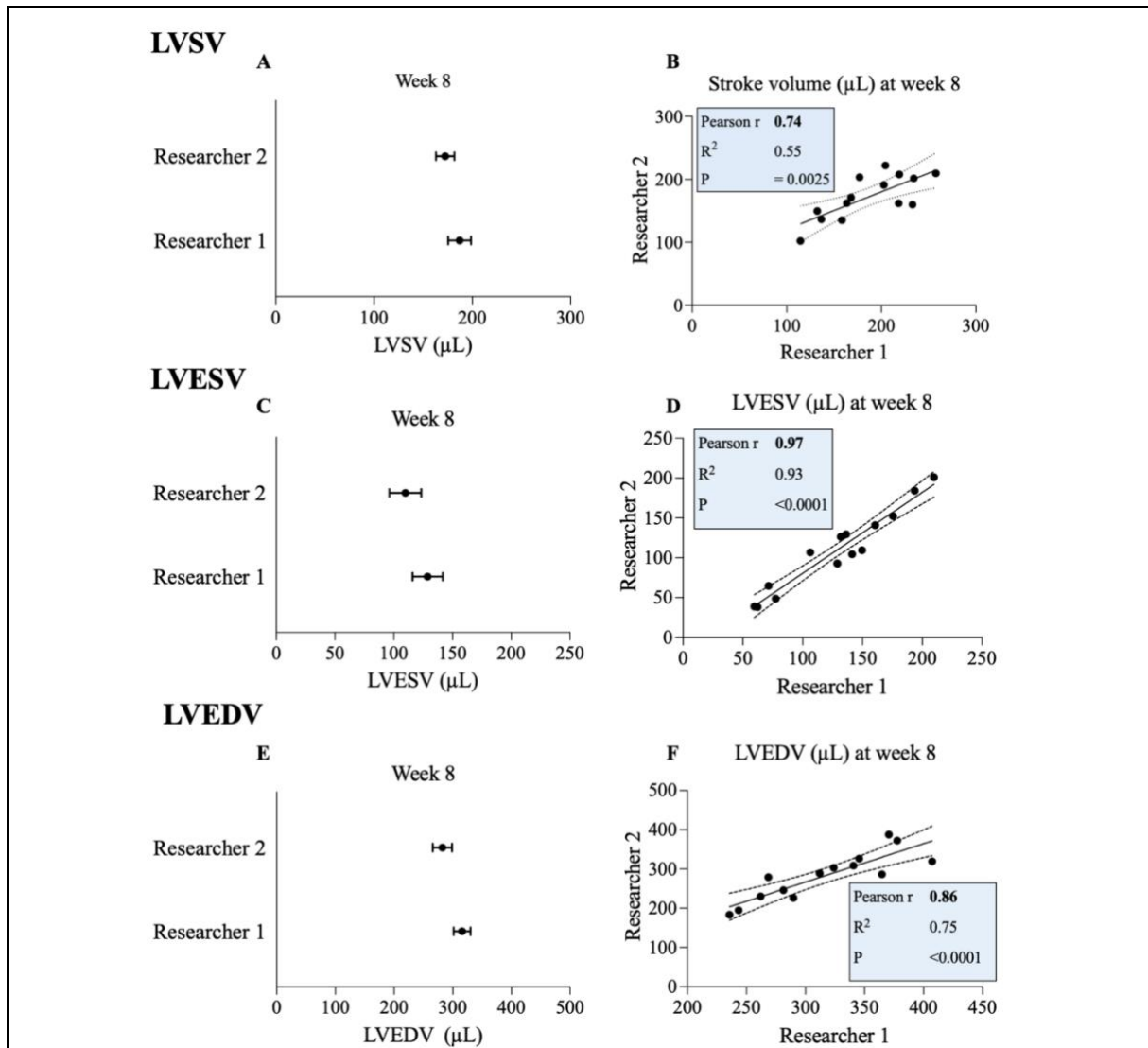
**Fig. 6 – Minimal variation observed between two researchers in volume measurements. (A-F)** Comparison between researchers 1 & 2 for LVESV **(A)**, LVEDV **(C)**, and LVSV **(E)**. Correlation between researchers 1 & 2 for LVESV **(B)**, LVEDV **(D)**, and LVSV **(F)**. All measurements were performed with DOX animals (N=14) 8 weeks after treatment. Data are represented as mean ± SEM. *p* <0.05. LVESV, Left ventricular end-systolic volume. LVEDV, Left ventricular end-diastolic volume. LVSV, Left ventricular stroke volume.

M-mode can be utilized to assess the systolic function and LV size by measuring the wall thickness. However, from parasternal views, it only provides information about two opposing myocardial walls, the anteroseptum and the posterior wall. Therefore, M-mode is not the preferred method due to its assumption of ellipsoid geometry for volumetric measurements (42, 57). B-mode generates 2D views of the heart (short or long axis). It enables the assessment of systolic and diastolic measurements along with indices of cardiac function such as LVCO, LVSV, LVEF, and LV volumes (42, 61). These parameters can be measured in both B-mode imaging views,

namely, single- and multiplane evaluation. Using the single plane of the parasternal long-axis, LV length at end-diastolic and end-systolic are measured to calculate the LVEDV and LVESV, based on these calculations, other systolic parameters can be determined. This imaging view is not preferred due to inaccuracy because of geometrical assumptions similar to M-mode. The multi-plane parasternal short-axis view enables more accurate and reliable measurement of ventricular volumes by using Simpson's biplane method. With this method, the total LV volume is determined by summing a series of elliptical discs from the apex of the heart to the base. Systolic and diastolic LV

volumes are calculated by using Simpson's rule (42, 61). For a more accurate assessment of cardiac volume and function without relying on geometrical assumptions, it is recommended to conduct 4DE. This modality enables the quantification of ventricular volumes and ensures an accurate EF% calculation. 4DE has certain benefits, including relatively low cost, rapid acquisition time, high spatial resolution, and strong agreement with CMR, which make it the first choice for correctly measuring LV systolic function and volumes (2, 42, 62). Zacchigna *et al.* recommend utilizing B-mode imaging to evaluate systolic function if 3D/4DE is unavailable. M-mode echocardiography should be restricted to measuring LV diameters and LVFS (42). Regarding systolic function, our results indicated that the different echocardiographic modalities provide comparable results when assessing LVEF and LVCO. The Bland-Altman plots for both parameters across the different echo modalities demonstrated a low bias, indicating a high level of reproducibility. For LVCO measurement, B-mode showed broad limits of agreement and higher bias than 4DE and M-mode, suggesting that B-mode exhibits greater variability in LVCO measurement. When comparing different echo modalities for volume parameters, significant differences in volumes emerged between B-mode and M-mode. For LVSV, LVESV, and LVEDV, the Bland-Altman plots exhibited the widest limits of agreement considering B-mode. Furthermore, comparing B-mode to 4DE, B-mode showed the highest bias among all modalities. In general, bias levels closer to zero indicate higher reproducibility. For B-mode, the bias for LVSV and LVESV was moderate, and LVEDV had a high bias, indicating low reproducibility. Moreover, volume measurements derived from B-mode tend to exhibit higher values than to those obtained through other modes. Altogether, these findings indicate that the data obtained from B-mode exhibit significant variability, rendering this technique less suitable for measuring volume function compared to 4DE and M-mode. Previous studies have demonstrated that 4DE significantly enhances the accuracy and reproducibility of LV function quantification when compared to B-mode echocardiography (56, 57, 63). This advanced imaging technique allows for real-time image analysis at multiple planes encompassing the LV. Global cardiac parameters such as LVEDV can be measured with fewer geometric assumptions than images acquired by 2D imaging, which is confirmed by our results; LVEDV measured with B-mode has the highest bias. 4DE uses ECG and respiratory gating to minimize motion artifacts during image reconstruction, leading to more consistent and reliable assessments of LV function (56). Nevertheless, the guidelines indicate that B-mode is preferable over M-mode echocardiography (42). However, our results demonstrate less variability and a higher reproducibility for M-mode than B-mode. This can be attributed to the greater complexity involved in analyzing B-mode echo images, which are manually assessed by two independent researchers. Furthermore, we used the single-plane parasternal long-axis view instead of the more accurate Simpson's method. Using Simpson's method could make our measurements of systolic and diastolic LV volumes more accurate and potentially improve the reproducibility and reliability of this modality in our study. The accuracy of B-mode echocardiography depends on the researcher's skill and experience in performing the echoes and the quality of the images. We suggest that different interpretations of the endocardial borders can lead to deviating and less reliable results. Therefore, in future studies, when assessing B-mode echocardiography, the use of Simpson's rule may help to address these limitations and enhance the diagnostic performance of B-mode echocardiography. Conversely, with single-dimensional imaging, M-mode echocardiography minimizes the complexity and variability associated with geometric assumptions despite providing less detailed information about the heart's function. Furthermore, research indicates that semi-automated contouring of the endocardial borders improves reproducibility in both 2DE and 3DE (64, 65). However, we did not have access to this semi-automated contouring program in our study.

*Strain measurement is not the most sufficient method for early detection in preclinical models* – Multiple preclinical studies have utilized speckle-tracing echocardiography (STE) to detect abnormalities in myocardial deformation to predict cardiotoxicity (48, 66-68). These studies showed that alternations in radial strain could detect changes in LV systolic function

induced by DOX treatment earlier than reductions observed in traditional echocardiographic parameters such as LVEF and LVFS. This indicates that radial strain could be an effective early marker for detecting myocardial dysfunction. In clinical practice, GLS is the most extensively studied and most important STE-derived parameter to detect myocardium deformation in humans. STE is broadly employed in clinics due to its sensitive and reproducible detection of local impairments in cardiac contractility and its lack of angle dependency. Moreover, it has been demonstrated that GLS can detect early LV dysfunction before measurable changes in LVEF occur (42, 55, 69, 70). Contrarily, while myocardial strain imaging has emerged as an important modality for early cardiotoxicity detection in humans, preclinical studies do not reflect this trend. This is because STE is not entirely angle-independent, while ultrasonic images normally have a higher resolution along the ultrasound beam compared with the perpendicular direction. Moreover, the accuracy of STE depends upon optimal image quality. Furthermore, values obtained in the parasternal long-axis view in rodents may lack precision compared to human studies. Additionally, without established reference values for animal models, a more comprehensive utilization of this technology is necessary to ensure reproducibility and accuracy in defining such standards (42, 71). Once STE application in rodent studies is optimized, better defined, and standardized, it should be incorporated into future studies as a sensitive method to early detect DOX-induced cardiotoxicity.

*Consistency in echocardiographic measurements between researchers* – Besides reproducibility of different echocardiographic modes, variation among researchers is also crucial for obtaining reliable results. Our data showed minimal variation between the systolic and volume measurements conducted by the two researchers. The study of Stegmann *et al.* showed an excellent agreement for inter-observer measurements with 4DE, confirming our results. Moreover, this study showed a higher inter-observer reproducibility of 4DE than to B-mode (57). This finding underscores the superiority of 4D imaging as the optimal approach for obtaining the most reliable results, even when different researchers perform the

scans. Only longitudinal LVFS showed a weak correlation between the measurements of the two researchers, suggesting substantial variation between the two researchers' measurements for this parameter. Nevertheless, longitudinal LVFS is determined using B-mode echocardiography. As previously mentioned, this method relies more on geometric assumptions, which makes this method more subjective. This subjectivity can lead to differences in interpretation and measurement among researchers. All together, these results underscore that B-mode echocardiography is suboptimal for cardiotoxicity detection. It emerges as the least reliable technique, compounded by significant interobserver variability.

*Limitations* – In contrast to cancer patients who developed DOX-induced cardiotoxicity and often have multiple comorbidities, the rats used in this study were healthy and free of any comorbid conditions. The shared risk factors between cancer and CVDs, such as obesity, smoking, and diabetes, and shared pathophysiological mechanisms, including oxidative stress and inflammation, render their interaction of significant interest (72, 73). Moreover, there is also an overlap between pathways essential for normal cardiac physiology and tumor growth. Consequently, these overlaps may elucidate the elevated risk of cardiotoxicity and HF associated with targeted anticancer treatments (72, 74). Therefore, using a healthy animal model may not fully replicate the complex physiological conditions and the reciprocal relationship between HF and cancer. Accordingly, a follow-up study with a tumor-induced rat model treated with DOX must be conducted to confirm our results. This study only includes echocardiographic measurements until the final DOX injection at week eight. Consequently, the evolution of cardiac function post-therapy could not be evaluated. The reproducibility of the different echocardiographic modes is only measured immediately after the last DOX injection. Ideally, a temporal variability test would be performed to assess the techniques across the periods. Minimizing temporal variability can improve the accuracy and consistency of echocardiographic evaluations to make sure that measurements truly represent cardiotoxicity (75).

15

## CONCLUSION

In conclusion, our study underscores the time-dependent manifestation of DOX-induced cardiotoxicity in a rat model, with discernible changes in LV systolic function and volumes becoming evident six weeks after a cumulative dose of 12 mg/kg DOX and intensifying after a cumulative dose of 16 mg/kg for eight weeks. Additionally, 4D-mode outperforms M-mode and B-mode echocardiography, suggesting 4DE as the method of choice for evaluating cardiotoxicity in rodents. Moreover, minimal variation was observed in systolic and volume measurements conducted by two researchers, ensuring excellent reliability. These findings underscore the importance of early cardiotoxicity detection and careful echocardiographic assessment with the most appropriate modality possible in DOX-induced cardiotoxicity rodent models. Ultimately, echocardiography remains an essential diagnostic technique for the real-time evaluation of cardiovascular function and early detection of DOX-induced cardiotoxicity.

## Practical work during my senior internship

My initial thesis project aimed to prove that pyridoxamine provides a cardioprotective effect in an orthotopic tumor-bearing rat model mimicking the clinical disease course of DOX-induced cardiotoxicity. Therefore, female Sprague Dawley rats were injected with cultured LA7 mammary cancer cells. Two weeks post-tumor induction, no palpable tumor was detected in our rat model. Despite optimization, significant results were not achieved, leading to the discontinuation of the study. Consequently, my practical work was shifted to a different study led by Ellen Heeren: 'How to mend a broken heart: combining CASCs with ELR hydrogel as a therapy to prevent progression from myocardial infarction to heart failure'. In this project, I utilized many techniques that are similar to those that would have been used in the initial project. This chapter provides an overview of the practical work carried out during my senior internship.

*Introduction* – CVD significantly impacts global health, being the leading cause of mortality and morbidity worldwide and accounting for approximately 18 million deaths each year (76). Myocardial infarction (MI), a common clinical manifestation of CVD, can quickly progress to HF by damaging the ventricular tissue. This damage is caused by the reduction or blockage of blood flow through the coronaries during MI and leads to dramatic and irreversible loss of cardiomyocytes (77). Due to the heart's limited regenerative capacity, the remaining cardiomyocytes are unable to regenerate and replace lost cells (78). Unfortunately, existing treatments for MI are insufficient to prevent its progression to HF. Stem cells have emerged as a promising approach to combat HF. Our research group has discovered a promising stem cell population, the Cardiac Atrial Appendage Stem Cells (CASCs), in the right atrial appendage of the heart. They can be identified based on their high aldehyde dehydrogenase (ALDH) enzyme activity (79). *In vitro* experiments have demonstrated that CASCs have a superior cardiomyogenic differentiation capacity compared to other types of cardiac stem cells (CSCs), making them particularly suitable for myocardial regeneration (80). Additionally, several *in vivo* studies showed that CASCs transplantation after MI preserved cardiac function by limiting cellular remodeling in a rat and minipig model, underscoring the therapeutic potential of CASCs in myocardial repair (81, 82). Nevertheless, after CASCs transplantation, the retention rate was only 19%, indicating that only one-fifth of the injected cells remained at the injection site. This is due to the stress conditions in the ischemic environment post-MI (82). The poor retention rate after transplantation hinders the restoration of cardiac function by preventing CASCs from integrating in the myocardium and differentiating into cardiomyocytes. This underscores the urgent need for an alternative strategy to enhance the retention rate and protect the CASCs after transplantation into the MI environment (82). Recently, an extracellular matrix (ECM)-mimicking hydrogel was used to improve cardiac function after MI (7). This elastin-like recombinamers (ELR) hydrogel facilitates a matrix-dependent modulation of the integrity and functionality of CSCs that persist following ischemia post-MI (83). Therefore, we propose that embedding CASCs in ELR hydrogel will increase their retention rate by providing support and protection for the cells and, consequently, restore cardiac

16

function after transplantation in the peri-infarct zone of an ischemia/reperfusion rat model for MI.

*Testing the compatibility of CASCs and ELR hydrogel* – In this study, we aimed to enhance the retention rate of CASCs by embedding them in an ELR hydrogel. This hydrogel was synthesized using catalyst-free click chemistry to cross-link two ELRs, namely HE5 and HRGD6 synthetic polypeptides. Moreover, the hydrogel features functional domains designed for cell adhesion and protease-sensitive cleavage sites, which are specifically cleavable by matrix metalloproteases that are overexpressed after MI. This design facilitates the biodegradation of the hydrogel, ensuring it provides essential support for the encapsulated cells during tissue regeneration and the formation of a new extracellular matrix (ECM). A previous study has demonstrated high viability of human foreskin fibroblasts in this ELR hydrogel (83). However, for the application with CASCs, it is crucial to establish that CASCs survive, proliferate, and migrate out of the hydrogel.

First, we had to optimize the coagulation of the ELR hydrogel for a 96-well and 24-well plate. Therefore, different concentrations of the components and various experimental setups were applied to coagulate the ELR hydrogel with and without CASCs. The optimal concentrations to coagulate the gel were for both components HE5 and HRGD6, 66,67mg/µL, wherein the gel comprises 25% CASCs or X-vivo medium, 57% HE5, and 18% HRGD6. Our results show that human and rat CASCs survive and proliferate in the ELR hydrogel. The following experimental setup was used to test the migration of CASCs in the hydrogel. CASCs were subjected to a starvation medium for two hours. Subsequently, they were harvested and resuspended in basal X-vivo medium with ELR hydrogel components to form a gel. A drop of this solution was dispensed in a 6-well plate. After coagulation, complete medium was added, and the hydrogel was placed in the IncuCyte live-cell imaging system to follow migration for ten days.

*Applying the CASCs-ELR combination therapy in vivo in a rat model for MI* – CASCs were isolated from the right appendage of

healthy eight-week-old female Sprague Dawley rats. First, we sacrificed the rats to isolate and perfuse the heart. The right atria of the heart tissue was then dissected, minced, and enzymatically digested. To specifically isolate CASCs, we used an Aldefluor staining, which targets ALDH-positive cells; this is a characteristic specific to CASCs. The mixture of right atria cells was sorted using flow cytometry, and CASCs were collected separately and cultured until they reached sufficient numbers for injection after approximately two weeks. Prior to surgery, baseline echocardiography was conducted to confirm the cardiac health of the animals at the start of the study. Therefore, the rats were shaved, and depilatory cream was applied to prevent hair-based artifacts. Rats were placed in a supine position, and parasternal long-axis and short-axis views at apical, mid-ventricular, and basal levels were acquired using M-mode and B-mode. Additionally, 4DE was performed, and the apical four-chamber view was used to perform pulsed wave Doppler imaging. At the same time, blood samples were collected from the lateral tail vein for later analysis. To establish the MI model, we permanently ligated the left anterior descending (LAD) coronary artery. The surgery was conducted as follows, left thoracotomy was performed in the third intercostal space to expose the heart. Afterward, the pericardium was opened, and the LAD was ligated. Successful ischemia was confirmed by observation of LV pallor immediately after ligation. Then, the chest was closed, and rats were extubated upon spontaneous respiration. The SHAM group underwent identical surgery without LAD ligation. One week after MI surgery, echocardiography was performed as described above, to confirm successful MI induction and to assess LVEF before injection with the respective therapies. To administer the therapy intramyocardially in the peri-infarct zone, echo-guided injection (EGI) was performed one week after MI surgery. Rats were randomly assigned to one of four MI groups: MI, MI with CASCs transplantation (MI + CASCs), MI with CASCs transplantation combined ELR hydrogel (MI + CASCs + H), and MI with only ELR hydrogel (MI + H) injection. Prior to EGI, ELR hydrogel was weighed and dissolved in basal X-VIVO medium overnight on ice. CASCs were harvested at passage two. For the CASCs therapy, $2 \times 10^6$ cells were dissolved in basal X-

vivo medium in a construct either containing Matrigel for the MI + CASCs group or hydrogel for the MI + CASCs + H group. In the MI + H group, ELR hydrogel was injected. Intramyocardial EGIs were performed with a total volume of 80μL in the anterior cardiac wall around the peri-infarct zone. Four weeks post-injection, echocardiography was performed to assess the effect of the respective therapies on cardiac function, and blood was taken as described above. To evaluate the effect of the respective therapies on LV pressure changes, invasive hemodynamic measurements were performed right before sacrifice. Five weeks post-MI, rats were sacrificed to harvest the hearts to perform histological and molecular analysis. Transversal sections were made of a segment of the LV that contained the transmural infarction, fixed in paraformaldehyde, embedded in paraffin, and sectioned for histological examination. The remaining LV tissue was snap-frozen in liquid nitrogen and crushed into a fine powder for molecular analysis, such as gene expression analysis.

My part in this *in vivo* study was to help with the CASCs isolation and maintenance and to prepare the different therapies for the EGI study. I prepared the rats for the echocardiography measurements by weighting, anesthetizing and shaving them, and took the blood samples. Moreover, I learned how to perform echocardiography and assisted with the MI operations and EGI injections. Lastly, I performed sacrifices and isolated the heart and organs. To discover the molecular mechanisms behind the CASCs hydrogel combination therapy, I checked gene expression in the isolated LV tissue for different hallmark genes of MI, such as genes for fibrosis, ROS, inflammation, and anoikis. First, interesting genes were searched, whereafter primers were designed, and qPCR was performed

**REFERENCES**

1. Christidi E, Brunham LR. Regulated cell death pathways in doxorubicin-induced cardiotoxicity. Cell Death & Disease. 2021;12(4):339.
2. O'Riordan CE, Trochet P, Steiner M, Fuchs D. Standardisation and future of preclinical echocardiography. Mamm Genome. 2023;34(2):123-55.
3. Dyba T, Randi G, Bray F, Martos C, Giusti F, Nicholson N, et al. The European cancer burden in 2020: Incidence and mortality estimates for 40 countries and 25 major cancers. Eur J Cancer. 2021;157:308-47.
4. Ferlay J, Colombet M, Soerjomataram I, Parkin DM, Piñeros M, Znaor A, et al. Cancer statistics for the year 2020: An overview. Int J Cancer. 2021.
5. Sung H, Ferlay J, Siegel RL, Laversanne M, Soerjomataram I, Jemal A, et al. Global Cancer Statistics 2020: GLOBOCAN Estimates of Incidence and Mortality Worldwide for 36 Cancers in 185 Countries. CA Cancer J Clin. 2021;71(3):209-49.
6. Nardin S, Mora E, Varughese FM, D'Avanzo F, Vachanaram AR, Rossi V, et al. Breast Cancer Survivorship, Quality of Life, and Late Toxicities. Front Oncol. 2020;10:864.
7. Galeş LN, Păun MA, Anghel RM, Trifănescu OG. Cancer Screening: Present Recommendations, the Development of Multi-Cancer Early Development Tests, and the Prospect of Universal Cancer Screening. Cancers (Basel). 2024;16(6).
8. Subhan MA, Parveen F, Shah H, Yalamarty SSK, Ataide JA, Torchilin VP. Recent Advances with Precision Medicine Treatment for Breast Cancer including Triple-Negative Sub-Type. Cancers (Basel). 2023;15(8).
9. Nicolazzi MA, Carnicelli A, Fuorlo M, Scaldaferri A, Masetti R, Landolfi R, et al. Anthracycline and trastuzumab-induced cardiotoxicity in breast cancer. Eur Rev Med Pharmacol Sci. 2018;22(7):2175-85.
10. Huang W, Xu R, Zhou B, Lin C, Guo Y, Xu H, et al. Clinical Manifestations, Monitoring, and Prognosis: A Review of Cardiotoxicity After Antitumor Strategy. Front Cardiovasc Med. 2022;9:912329.
11. McGowan JV, Chung R, Maulik A, Piotrowska I, Walker JM, Yellon DM. Anthracycline Chemotherapy and Cardiotoxicity. Cardiovasc Drugs Ther. 2017;31(1):63-75.
12. Zamorano JL, Lancellotti P, Rodriguez Muñoz D, Aboyans V, Asteggiano R, Galderisi M, et al. 2016 ESC Position Paper on cancer treatments and cardiovascular toxicity developed under the auspices of the ESC Committee for Practice Guidelines: The Task Force for cancer treatments and cardiovascular toxicity of the European Society of Cardiology (ESC). Eur Heart J. 2016;37(36):2768-801.
13. Cardinale D, Iacopo F, Cipolla CM. Cardiotoxicity of Anthracyclines. Front Cardiovasc Med. 2020;7:26.
14. Patnaik JL, Byers T, DiGuiseppi C, Dabelea D, Denberg TD. Cardiovascular disease competes with breast cancer as the leading cause of death for older females diagnosed with breast cancer: a retrospective cohort study. Breast Cancer Res. 2011;13(3):R64.
15. Sturgeon KM, Deng L, Bluethmann SM, Zhou S, Trifiletti DM, Jiang C, et al. A population-based study of cardiovascular disease mortality risk in US cancer patients. Eur Heart J. 2019;40(48):3889-97.
16. Strongman H, Gadd S, Matthews AA, Mansfield KE, Stanway S, Lyon AR, et al. Does Cardiovascular Mortality Overtake Cancer Mortality During Cancer Survivorship?: An English Retrospective Cohort Study. JACC CardioOncol. 2022;4(1):113-23.
17. Linders AN, Dias IB, López Fernández T, Tocchetti CG, Bomer N, Van der Meer P. A review of the pathophysiological mechanisms of doxorubicin-induced cardiotoxicity and aging. npj Aging. 2024;10(1):9.
18. Saleh Y, Abdelkarim O, Herzallah K, Abela GS. Anthracycline-induced cardiotoxicity: mechanisms of action, incidence, risk factors, prevention, and treatment. Heart Fail Rev. 2021;26(5):1159-73.
19. Sala V, Della Sala A, Hirsch E, Ghigo A. Signaling Pathways Underlying Anthracycline Cardiotoxicity. Antioxid Redox Signal. 2020;32(15):1098-114.
20. Sawyer DB. Anthracyclines and heart failure. N Engl J Med. 2013;368(12):1154-6.

21. Songbo M, Lang H, Xinyong C, Bin X, Ping Z, Liang S. Oxidative stress injury in doxorubicin-induced cardiotoxicity. Toxicol Lett. 2019;307:41-8.

22. Angsutararux P, Luanpitpong S, Issaragrisil S. Chemotherapy-Induced Cardiotoxicity: Overview of the Roles of Oxidative Stress. Oxid Med Cell Longev. 2015;2015:795602.

23. Nebigil CG, Désaubry L. Updates in Anthracycline-Mediated Cardiotoxicity. Frontiers in Pharmacology. 2018;9.

24. Bayles CE, Hale DE, Konieczny A, Anderson VD, Richardson CR, Brown KV, et al. Upcycling the anthracyclines: New mechanisms of action, toxicology, and pharmacology. Toxicol Appl Pharmacol. 2023;459:116362.

25. Kong CY, Guo Z, Song P, Zhang X, Yuan YP, Teng T, et al. Underlying the Mechanisms of Doxorubicin-Induced Acute Cardiotoxicity: Oxidative Stress and Cell Death. Int J Biol Sci. 2022;18(2):760-70.

26. Truong J, Yan AT, Cramarossa G, Chan KK. Chemotherapy-induced cardiotoxicity: detection, prevention, and management. Can J Cardiol. 2014;30(8):869-78.

27. Kourek C, Touloupaki M, Rempakos A, Loritis K, Tsougkos E, Paraskevaidis I, et al. Cardioprotective Strategies from Cardiotoxicity in Cancer Patients: A Comprehensive Review. J Cardiovasc Dev Dis. 2022;9(8).

28. Ewer MS, Ewer SM. Cardiotoxicity of anticancer treatments. Nature Reviews Cardiology. 2015;12(9):547-58.

29. Vejpongsa P, Yeh ET. Prevention of anthracycline-induced cardiotoxicity: challenges and opportunities. J Am Coll Cardiol. 2014;64(9):938-45.

30. Menna P, Salvatorelli E. Primary Prevention Strategies for Anthracycline Cardiotoxicity: A Brief Overview. Chemotherapy. 2017;62(3):159-68.

31. Macedo AVS, Hajjar LA, Lyon AR, Nascimento BR, Putzu A, Rossi L, et al. Efficacy of Dexrazoxane in Preventing Anthracycline Cardiotoxicity in Breast Cancer. JACC CardioOncol. 2019;1(1):68-79.

32. Henriksen PA. Anthracycline cardiotoxicity: an update on mechanisms, monitoring and prevention. Heart. 2018;104(12):971-7.

33. Hahn VS, Lenihan DJ, Ky B. Cancer therapy-induced cardiotoxicity: basic mechanisms and potential cardioprotective therapies. J Am Heart Assoc. 2014;3(2):e000665.

34. Zhang J, Li X, Liu J, Shang Y, Tan L, Guo Y. Early and dynamic detection of doxorubicin induced cardiotoxicity by myocardial contrast echocardiography combined with two-dimensional speckle tracking echocardiography in rats. Front Cardiovasc Med. 2022;9:1063499.

35. Bikiewicz A, Banach M, von Haehling S, Maciejewski M, Bielecka-Dabrowa A. Adjuvant breast cancer treatments cardiotoxicity and modern methods of detection and prevention of cardiac complications. ESC Heart Fail. 2021;8(4):2397-418.

36. Čelutkienė J, Pudil R, López-Fernández T, Grapsa J, Nihoyannopoulos P, Bergler-Klein J, et al. Role of cardiovascular imaging in cancer patients receiving cardiotoxic therapies: a position statement on behalf of the Heart Failure Association (HFA), the European Association of Cardiovascular Imaging (EACVI) and the Cardio-Oncology Council of the European Society of Cardiology (ESC). Eur J Heart Fail. 2020;22(9):1504-24.

37. Marwick TH. Global Longitudinal Strain Monitoring to Guide Cardioprotective Medications During Anthracycline Treatment. Curr Oncol Rep. 2022;24(6):687-94.

38. Bloom MW, Hamo CE, Cardinale D, Ky B, Nohria A, Baer L, et al. Cancer Therapy-Related Cardiac Dysfunction and Heart Failure: Part 1: Definitions, Pathophysiology, Risk Factors, and Imaging. Circ Heart Fail. 2016;9(1):e002661.

39. Levis BE, Binkley PF, Shapiro CL. Cardiotoxic effects of anthracycline-based therapy: what is the evidence and what are the potential harms? Lancet Oncol. 2017;18(8):e445-e56.

40. Nonaka M, Hosoda H, Uezono Y. Cancer treatment-related cardiovascular disease: Current status and future research priorities. Biochem Pharmacol. 2021;190:114599.

41. de Baat EC, Naaktgeboren WR, Leiner T, Teske AJ, Habets J, Grotenhuis HB. Update in imaging of cancer therapy-related cardiac toxicity in adults. Open Heart. 2021;8(1).

42. Zacchigna S, Paldino A, Falcão-Pires I, Daskalopoulos EP, Dal Ferro M, Vodret S, et al. Towards standardization of echocardiography for the evaluation of left ventricular function in adult

rodents: a position paper of the ESC Working Group on Myocardial Function. Cardiovascular Research. 2020;117(1):43-59.

43.     Asnani A, Moslehi JJ, Adhikari BB, Baik AH, Beyer AM, de Boer RA, et al. Preclinical Models of Cancer Therapy-Associated Cardiovascular Toxicity: A Scientific Statement From the American Heart Association. Circ Res. 2021;129(1):e21-e34.

44.     Bunting KV, Steeds RP, Slater K, Rogers JK, Gkoutos GV, Kotecha D. A Practical Guide to Assess the Reproducibility of Echocardiographic Measurements. J Am Soc Echocardiogr. 2019;32(12):1505-15.

45.     Nair AB, Jacob S. A simple practice guide for dose conversion between animals and human. J Basic Clin Pharm. 2016;7(2):27-31.

46.     Chang HM, Moudgil R, Scarabelli T, Okwuosa TM, Yeh ETH. Cardiovascular Complications of Cancer Therapy: Best Practices in Diagnosis, Prevention, and Management: Part 1. J Am Coll Cardiol. 2017;70(20):2536-51.

47.     Chan BYH, Roczkowsky A, Cho WJ, Poirier M, Sergi C, Keschrumrus V, et al. MMP inhibitors attenuate doxorubicin cardiotoxicity by preventing intracellular and extracellular matrix remodelling. Cardiovascular Research. 2020;117(1):188-200.

48.     Kang Y, Wang W, Zhao H, Qiao Z, Shen X, He B. Assessment of Subclinical Doxorubicin-induced Cardiotoxicity in a Rat Model by Speckle-Tracking Imaging. Arq Bras Cardiol. 2017;109(2):0.

49.     Xiang P, Deng HY, Li K, Huang G-Y, Chen Y, Tu L, et al. Dexrazoxane protects against doxorubicin-induced cardiomyopathy: upregulation of Akt and Erk phosphorylation in a rat model. Cancer Chemotherapy and Pharmacology. 2009;63(2):343-9.

50.     Bertinchant JP, Polge A, Juan JM, Oliva-Lauraire MC, Giuliani I, Marty-Double C, et al. Evaluation of cardiac troponin I and T levels as markers of myocardial damage in doxorubicin-induced cardiomyopathy rats, and their relationship with echocardiographic and histological findings. Clinica Chimica Acta. 2003;329(1):39-51.

51.     Chakouri N, Farah C, Matecki S, Amedro P, Vincenti M, Saumet L, et al. Screening for in-vivo regional contractile defaults to predict the delayed Doxorubicin Cardiotoxicity in Juvenile Rat. Theranostics. 2020;10(18):8130-42.

52.     Ohlig J, Henninger C, Zander S, Merx M, Kelm M, Fritz G. Rac1-mediated cardiac damage causes diastolic dysfunction in a mouse model of subacute doxorubicin-induced cardiotoxicity. Archives of Toxicology. 2018;92(1):441-53.

53.     McLean BA, Patel VB, Zhabyeyev P, Chen X, Basu R, Wang F, et al. PI3Kα Pathway Inhibition With Doxorubicin Treatment Results in Distinct Biventricular Atrophy and Remodeling With Right Ventricular Dysfunction. J Am Heart Assoc. 2019;8(9):e010961.

54.     Mincu RI, Lampe LF, Mahabadi AA, Kimmig R, Rassaf T, Totzeck M. Left Ventricular Diastolic Function Following Anthracycline-Based Chemotherapy in Patients with Breast Cancer without Previous Cardiac Disease-A Meta-Analysis. J Clin Med. 2021;10(17).

55.     Plana JC, Galderisi M, Barac A, Ewer MS, Ky B, Scherrer-Crosbie M, et al. Expert consensus for multimodality imaging evaluation of adult patients during and after cancer therapy: a report from the American Society of Echocardiography and the European Association of Cardiovascular Imaging. J Am Soc Echocardiogr. 2014;27(9):911-39.

56.     Rutledge C, Cater G, McMahon B, Guo L, Nouraie SM, Wu Y, et al. Commercial 4-dimensional echocardiography for murine heart volumetric evaluation after myocardial infarction. Cardiovasc Ultrasound. 2020;18(1):9.

57.     Stegmann H, Bäuerle T, Kienle K, Dittrich S, Alkassar M. 4D cardiac magnetic resonance imaging, 4D and 2D transthoracic echocardiography: a comparison of in-vivo assessment of ventricular function in rats. Lab Anim. 2019;53(2):169-79.

58.     Bertinchant JP, Polge A, Juan JM, Oliva-Lauraire MC, Giuliani I, Marty-Double C, et al. Evaluation of cardiac troponin I and T levels as markers of myocardial damage in doxorubicin-induced cardiomyopathy rats, and their relationship with echocardiographic and histological findings. Clin Chim Acta. 2003;329(1-2):39-51.

59.     Podyacheva EY, Kushnareva EA, Karpov AA, Toropova YG. Analysis of Models of Doxorubicin-Induced Cardiomyopathy in Rats and Mice. A Modern View From the Perspective of the Pathophysiologist and the Clinician. Front Pharmacol. 2021;12:670479.

60.     Grune J, Blumrich A, Brix S, Jeuthe S, Drescher C, Grune T, et al. Evaluation of a commercial multi-dimensional echocardiography technique for ventricular volumetry in small animals. Cardiovasc Ultrasound. 2018;16(1):10.

61.     Lindsey ML, Kassiri Z, Virag JAI, de Castro Brás LE, Scherrer-Crosbie M. Guidelines for measuring cardiac physiology in mice. Am J Physiol Heart Circ Physiol. 2018;314(4):H733-h52.

62.     Moran CM, Thomson AJ, Rog-Zielinska E, Gray GA. High-resolution echocardiography in the assessment of cardiac physiology and disease in preclinical models. Exp Physiol. 2013;98(3):629-44.

63.     Chen R, Zhu M, Sahn DJ, Ashraf M. Non-Invasive Evaluation of Heart Function with Four-Dimensional Echocardiography. PLoS One. 2016;11(5):e0154996.

64.     Muraru D, Badano LP, Piccoli G, Gianfagna P, Del Mestre L, Ermacora D, et al. Validation of a novel automated border-detection algorithm for rapid and accurate quantitation of left ventricular volumes based on three-dimensional echocardiography. Eur J Echocardiogr. 2010;11(4):359-68.

65.     Cannesson M, Tanabe M, Suffoletto MS, McNamara DM, Madan S, Lacomis JM, et al. A novel two-dimensional echocardiographic image analysis system using artificial intelligence-learned pattern recognition for rapid automated ejection fraction. J Am Coll Cardiol. 2007;49(2):217-26.

66.     Coppola C, Riccio G, Barbieri A, Monti MG, Piscopo G, Rea D, et al. Antineoplastic-related cardiotoxicity, morphofunctional aspects in a murine model: contribution of the new tool 2D-speckle tracking. Onco Targets Ther. 2016;9:6785-94.

67.     Rea D, Coppola C, Barbieri A, Monti MG, Misso G, Palma G, et al. Strain Analysis in the Assessment of a Mouse Model of Cardiotoxicity due to Chemotherapy: Sample for Preclinical Research. In Vivo. 2016;30(3):279-90.

68.     Burdick J, Berridge B, Coatney R. Strain echocardiography combined with pharmacological stress test for early detection of anthracycline induced cardiomyopathy. J Pharmacol Toxicol Methods. 2015;73:15-20.

69.     Dobson R, Ghosh AK, Ky B, Marwick T, Stout M, Harkness A, et al. BSE and BCOS Guideline for Transthoracic Echocardiographic Assessment of Adult Cancer Patients Receiving Anthracyclines and/or Trastuzumab. JACC CardioOncol. 2021;3(1):1-16.

70.     Zito C, Longobardo L, Cadeddu C, Monte I, Novo G, Dell'Oglio S, et al. Cardiovascular imaging in the diagnosis and monitoring of cardiotoxicity: role of echocardiography. J Cardiovasc Med (Hagerstown). 2016;17 Suppl 1:S35-44.

71.     Mor-Avi V, Lang RM, Badano LP, Belohlavek M, Cardim NM, Derumeaux G, et al. Current and evolving echocardiographic techniques for the quantitative evaluation of cardiac mechanics: ASE/EAE consensus statement on methodology and indications endorsed by the Japanese Society of Echocardiography. J Am Soc Echocardiogr. 2011;24(3):277-313.

72.     de Wit S, Glen C, de Boer RA, Lang NN. Mechanisms shared between cancer, heart failure, and targeted anti-cancer therapies. Cardiovasc Res. 2023;118(18):3451-66.

73.     Guler MN, Tscheiller NM, Sabater-Molina M, Gimeno JR, Nebigil CG. Evidence for reciprocal network interactions between injured hearts and cancer. Front Cardiovasc Med. 2022;9:929259.

74.     Bertero E, Ameri P, Maack C. Bidirectional Relationship Between Cancer and Heart Failure: Old and New Issues in Cardio-oncology. Card Fail Rev. 2019;5(2):106-11.

75.     Thavendiranathan P, Grant AD, Negishi T, Plana JC, Popović ZB, Marwick TH. Reproducibility of echocardiographic techniques for sequential assessment of left ventricular ejection fraction and volumes: application to patients undergoing cancer chemotherapy. J Am Coll Cardiol. 2013;61(1):77-84.

76.     World Health Organization. Cardiovascular diseases 2021, visited on 29/05/2024, [Available from: https://www.who.int/health-topics/cardiovascular-diseases/#tab=tab_1.]

77.     He L, Nguyen NB, Ardehali R, Zhou B. Heart Regeneration by Endogenous Stem Cells and Cardiomyocyte Proliferation: Controversy, Fallacy, and Progress. Circulation. 2020;142(3):275-91.

78.     Hendrikx M, Hensen K, Clijsters C, Jongen H, Koninckx R, Bijnens E, et al. Recovery of regional but not global contractile function by the direct intramyocardial autologous bone marrow transplantation: results from a randomized controlled clinical trial. Circulation. 2006;114(1 Suppl):I101-7.

79.     Koninckx R, Daniëls A, Windmolders S, Mees U, Macianskiene R, Mubagwa K, et al. The cardiac atrial appendage stem cell: a new and promising candidate for myocardial repair. Cardiovasc Res. 2013;97(3):413-23.

80.      Koninckx R, Daniëls A, Windmolders S, Mees U, Macianskiene R, Mubagwa K, et al. The cardiac atrial appendage stem cell: a new and promising candidate for myocardial repair. Cardiovascular Research. 2012;97(3):413-23.

81.      Evens L, Beliën H, D'Haese S, Haesen S, Verboven M, Rummens JL, et al. Combinational Therapy of Cardiac Atrial Appendage Stem Cells and Pyridoxamine: The Road to Cardiac Repair? Int J Mol Sci. 2021;22(17).

82.      Fanton Y, Robic B, Rummens JL, Daniëls A, Windmolders S, Willems L, et al. Cardiac atrial appendage stem cells engraft and differentiate into cardiomyocytes in vivo: A new tool for cardiac repair after MI. Int J Cardiol. 2015;201:10-9.

83.      Contessotto P, Orbanić D, Da Costa M, Jin C, Owens P, Chantepie S, et al. Elastin-like recombinamers-based hydrogel modulates post-ischemic remodeling in a non-transmural myocardial infarction in sheep. Sci Transl Med. 2021;13(581).

*This text was supported by OpenAI.*

*Author contributions* – VB, DD, and SH conceived and designed the research. SH and DD conducted experiments. SH, DD, and LS performed data analysis. LS wrote the paper. SH carefully revised and approved the manuscript. EH supervised the practical part of the senior internship and reviewed this chapter in the manuscript.

**SUPPLEMENTARY FIGURES**
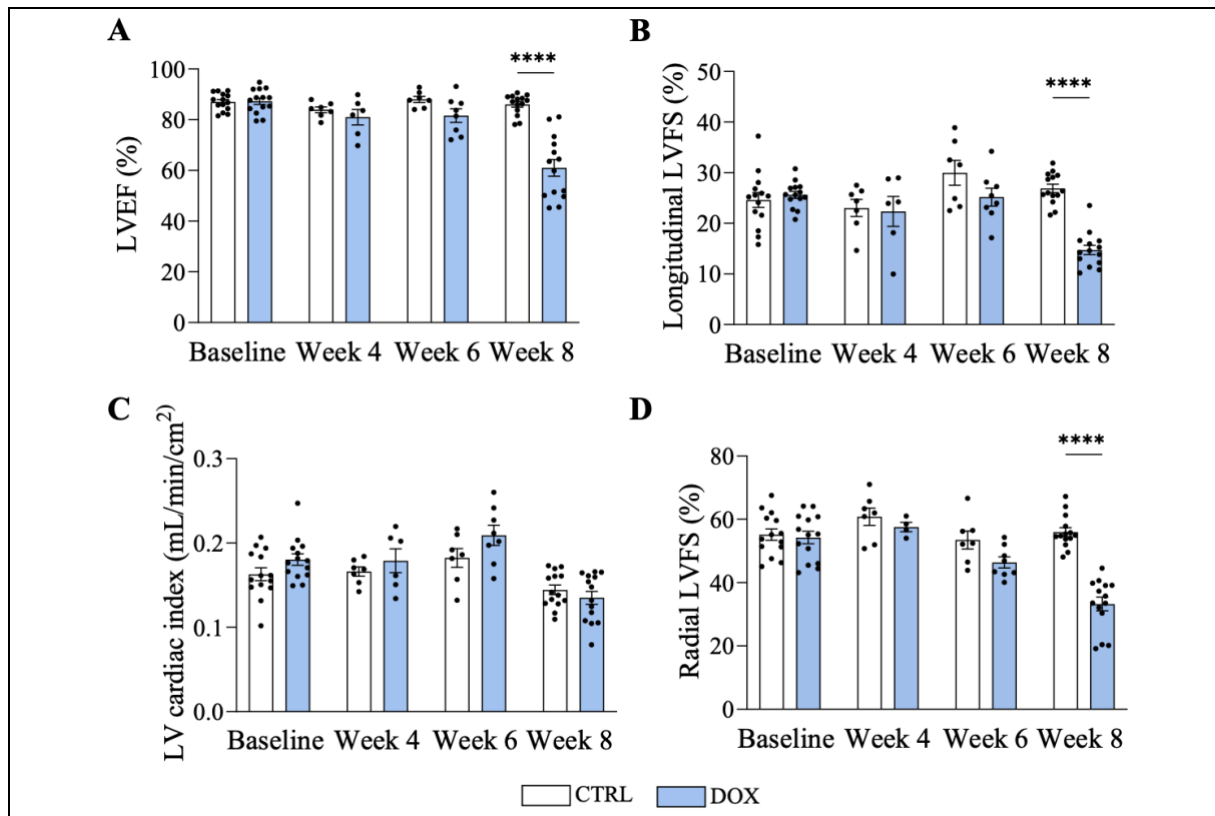


**Fig. S1 – DOX reduces systolic function after eight weeks. (A-D)** Percentage of LVEF **(A)**, percentage of longitudinal LVFS **(B)**, cardiac index **(C)**, and percentage of radial LVFS **(D),** at baseline, weeks 4, 6, and 8 in CTRL (CTRL, N=14) and DOX (DOX, N=14) animals. LVEF and cardiac index were measured with 4D-mode. Longitudinal and radial LVFS were measured with PSLAX B-mode and PSSAX M-mode, respectively. The cardiac index was determined by normalizing the cardiac output to the body surface area (BSA). Data are represented as mean ± SEM. *p<0.05, **p<0.01, ***p<0.001, ****p<0.0001. ns, not significant. LV, left ventricle. LVEF, left ventricular ejection fraction. LVFS, left ventricular fractional shortening.
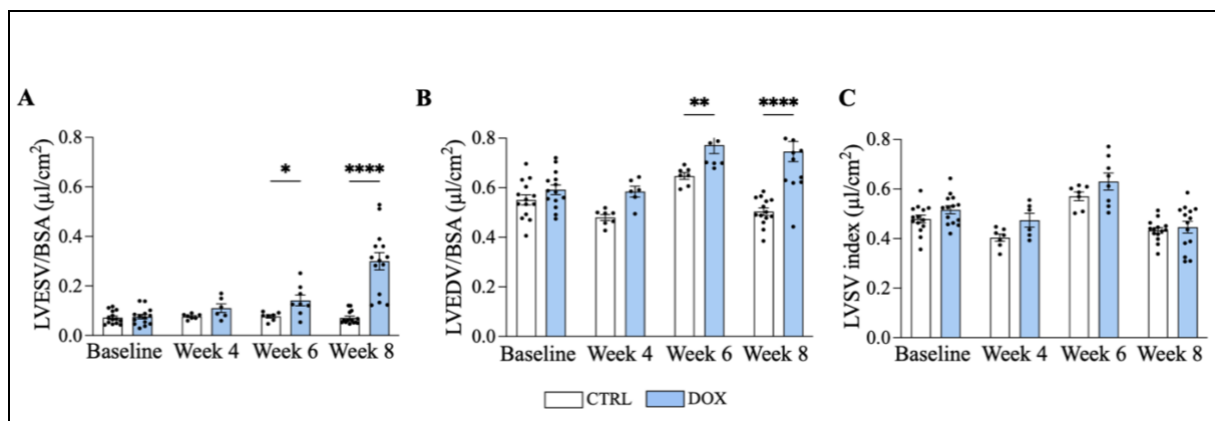


**Fig. S2 – ESV and EDV increased after six weeks in DOX-treated animals. (A-C)** ESV/BSA **(A)**, EDV/BSA **(B)**, and SV index **(C)** at baseline, weeks 4, 6, and 8 in CTRL (CTRL, N=14) and DOX (DOX, N=14) animals. ESV, EDV, and stroke volume index were measured with 4D-mode. The stroke volume index represents by stroke volume normalized to the body surface area (BSA). ESV, and EDV were normalized to BSA. Data are represented as mean ± SEM. *p<0.05, **p<0.01, ***p<0.001, ****p<0.0001. ns, not significant. ESV, end-systolic volume. EDV, end-diastolic volume. SV, stroke volume
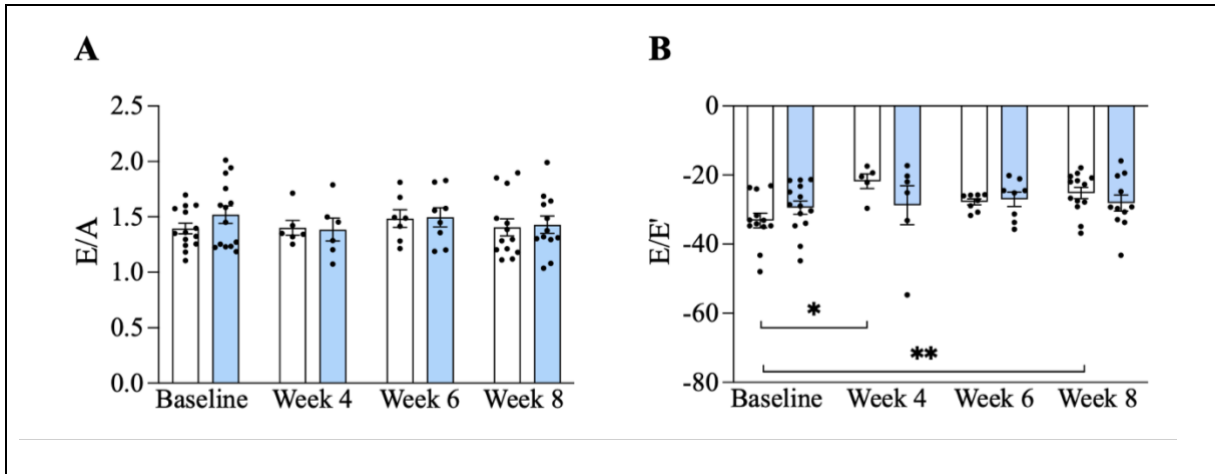
**Fig. S3 – DOX cardiotoxicity does not change diastolic function. (A-B)** E/A **(A)**, and E/E' **(B)** at baseline, weeks 4, 6, and 8 in CTRL (CTRL, N=14) and DOX (DOX, N=14) animals. Data are represented as mean ± SEM. *$p<0.05$, **$p<0.01$. A mitral flow velocity in the late filling phase. E, mitral flow velocity in the early filling phase. E', peak septal mitral annulus velocity in the early filling phase.
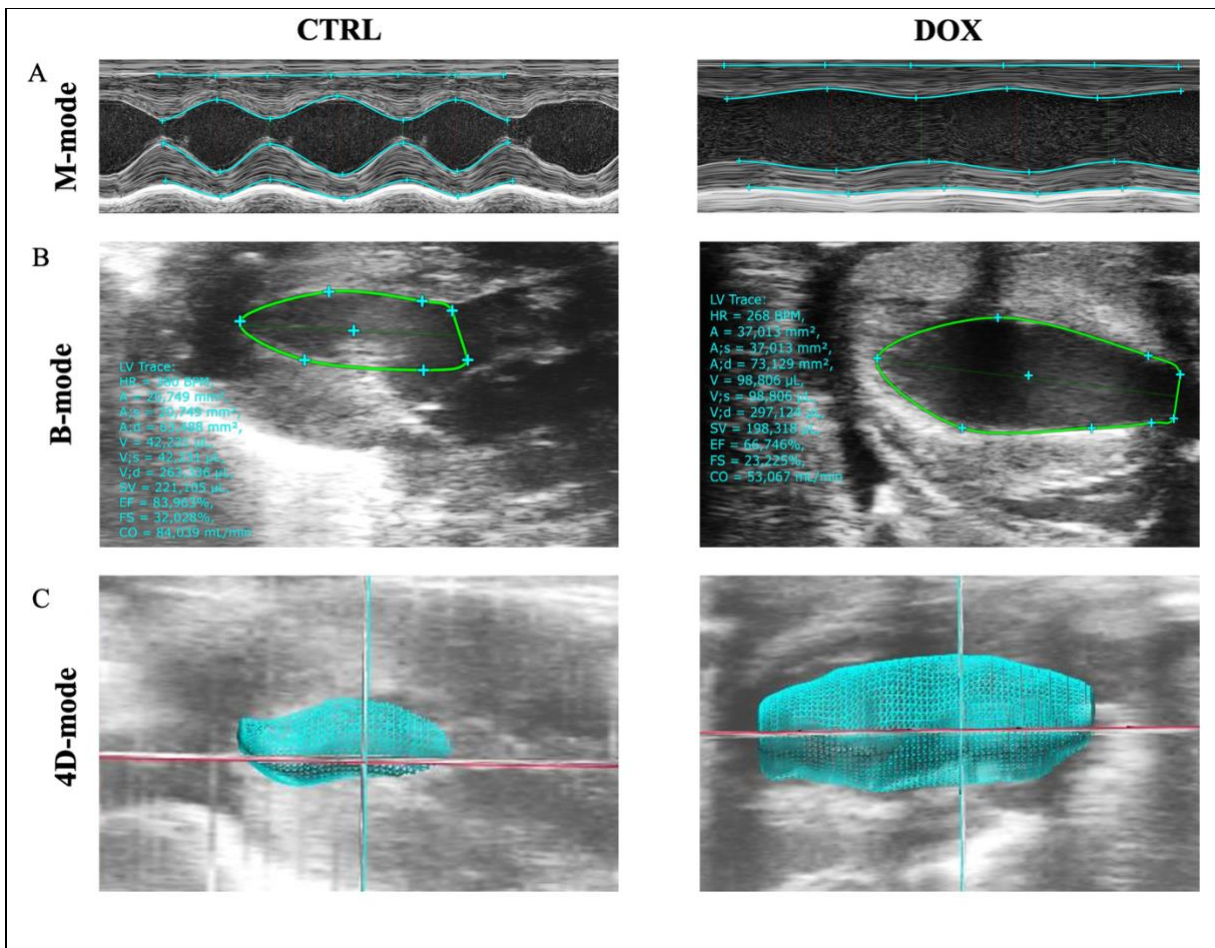


**Fig. S4 – Representative echocardiographic images at week 8.** Representative images of M-mode obtained during parasternal short-axis view at mid-ventricular level with LV trace **(A)**, B-mode during systole obtained during parasternal long-axis view at mid-ventricular level with LV trace **(B)**, 4D reconstructed hearts during systole **(C)** at week 8 of CTRL and DOX.